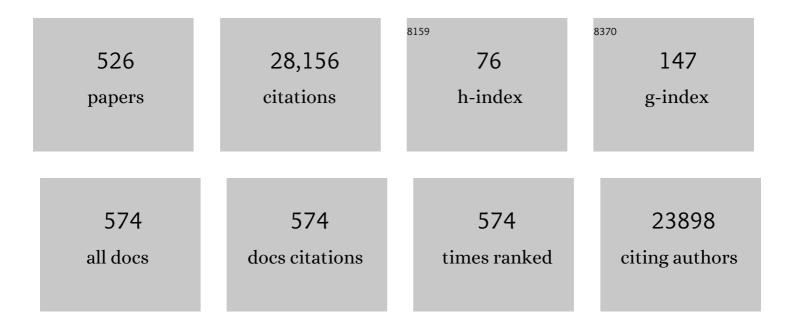
List of Publications by Year in descending order

Source: https://exaly.com/author-pdf/2544654/publications.pdf Version: 2024-02-01



#	Article	IF	CITATIONS
1	Study of ⁸⁹ Zr-Pembrolizumab PET/CT in Patients With Advanced-Stage Non–Small Cell Lung Cancer. Journal of Nuclear Medicine, 2022, 63, 362-367.	2.8	44
2	Quantitative Radiomics Features in Diffuse Large B-Cell Lymphoma: Does Segmentation Method Matter?. Journal of Nuclear Medicine, 2022, 63, 389-395.	2.8	16
3	18F-FDG PET baseline radiomics features improve the prediction of treatment outcome in diffuse large B-cell lymphoma. European Journal of Nuclear Medicine and Molecular Imaging, 2022, 49, 932-942.	3.3	62
4	A Guide to ComBat Harmonization of Imaging Biomarkers in Multicenter Studies. Journal of Nuclear Medicine, 2022, 63, 172-179.	2.8	96
5	¹⁸ F-FDG PET Improves Baseline Clinical Predictors of Response in Diffuse Large B-Cell Lymphoma: The HOVON-84 Study. Journal of Nuclear Medicine, 2022, 63, 1001-1007.	2.8	12
6	Early Response Prediction of Multiparametric Functional MRI and 18F-FDG-PET in Patients with Head and Neck Squamous Cell Carcinoma Treated with (Chemo)Radiation. Cancers, 2022, 14, 216.	1.7	14
7	Differential associations between neocortical tau pathology and blood flow with cognitive deficits in early-onset vs late-onset Alzheimer's disease. European Journal of Nuclear Medicine and Molecular Imaging, 2022, 49, 1951-1963.	3.3	8
8	The Impact of Semiautomatic Segmentation Methods on Metabolic Tumor Volume, Intensity, and Dissemination Radiomics in ¹⁸ F-FDG PET Scans of Patients with Classical Hodgkin Lymphoma. Journal of Nuclear Medicine, 2022, 63, 1424-1430.	2.8	20
9	Validation and test–retest repeatability performance of parametric methods for [11C]UCB-J PET. EJNMMI Research, 2022, 12, 3.	1.1	3
10	Influences on PET Quantification and Interpretation. Diagnostics, 2022, 12, 451.	1.3	9
11	Targeting PSMA Revolutionizes the Role of Nuclear Medicine in Diagnosis and Treatment of Prostate Cancer. Cancers, 2022, 14, 1169.	1.7	15
12	3D Convolutional Neural Network-Based Denoising of Low-Count Whole-Body 18F-Fluorodeoxyglucose and 89Zr-Rituximab PET Scans. Diagnostics, 2022, 12, 596.	1.3	1
13	Noise sensitivity of 89Zr-Immuno-PET radiomics based on count-reduced clinical images. EJNMMI Physics, 2022, 9, 16.	1.3	3
14	Standardised uptake values as determined on prostateâ€specific membrane antigen positron emission tomography/computed tomography is associated with oncological outcomes in patients with prostate cancer. BJU International, 2022, 129, 768-776.	1.3	7
15	Proposed New Dynamic Prognostic Index for Diffuse Large B-Cell Lymphoma: International Metabolic Prognostic Index. Journal of Clinical Oncology, 2022, 40, 2352-2360.	0.8	53
16	First-time imaging of [89Zr]trastuzumab in breast cancer using a long axial field-of-view PET/CT scanner. European Journal of Nuclear Medicine and Molecular Imaging, 2022, 49, 3593-3595.	3.3	11
17	Effects of Tracer Uptake Time in Non–Small Cell Lung Cancer ¹⁸ F-FDG PET Radiomics. Journal of Nuclear Medicine, 2022, 63, 919-924.	2.8	6
18	EANM procedure guidelines for brain PET imaging using [18F]FDG, version 3. European Journal of Nuclear Medicine and Molecular Imaging, 2022, 49, 632-651.	3.3	82

#	Article	IF	CITATIONS
19	Prediction of Non-Response to Neoadjuvant Chemoradiotherapy in Esophageal Cancer Patients with 18F-FDG PET Radiomics Based Machine Learning Classification. Diagnostics, 2022, 12, 1070.	1.3	7
20	Glioma perfusion quantification with ASL and DSC: head-to-head comparison with 15O-H2O PET. Nuklearmedizin - NuclearMedicine, 2022, 61, .	0.3	0
21	Metabolic Tumor Volume for Outcome Prediction in Patients with Aggressive B-Cell Lymphoma Undergoing Chimeric Antigen Receptor T-Cell Therapy. Nuklearmedizin - NuclearMedicine, 2022, 61, .	0.3	Ο
22	Bloodâ€circulating EVâ€miRNAs, serum TARC, and quantitative FDGâ€PET features in classical Hodgkin lymphoma. EJHaem, 2022, 3, 908-912.	0.4	2
23	Quality control in PET/CT and PET/MRI: Results of a survey amongst European countries. Physica Medica, 2022, 99, 16-21.	0.4	5
24	Functional stress imaging to predict abnormal coronary fractional flow reserve: the PACIFIC 2 study. European Heart Journal, 2022, 43, 3118-3128.	1.0	26
25	Alzheimer's disease pattern derived from relative cerebral flow as an alternative for the metabolic pattern using SSM/PCA. EJNMMI Research, 2022, 12, .	1.1	4
26	Detection of prostate cancer with 18F-DCFPyL PET/CT compared to final histopathology of radical prostatectomy specimens: is PSMA-targeted biopsy feasible? The DeTeCT trial. World Journal of Urology, 2021, 39, 2439-2446.	1.2	26
27	Repeatability of parametric methods for [¹⁸ F]florbetapir imaging in Alzheimer's disease and healthy controls: A test–retest study. Journal of Cerebral Blood Flow and Metabolism, 2021, 41, 569-578.	2.4	10
28	Simulating the effect of cerebral blood flow changes on regional quantification of [¹⁸ F]flutemetamol and [¹⁸ F]florbetaben studies. Journal of Cerebral Blood Flow and Metabolism, 2021, 41, 579-589.	2.4	12
29	Pelvic lymph-node staging with 18F-DCFPyL PET/CT prior to extended pelvic lymph-node dissection in primary prostate cancer - the SALT trial European Journal of Nuclear Medicine and Molecular Imaging, 2021, 48, 509-520.	3.3	60
30	Machine learning-based analysis of [18F]DCFPyL PET radiomics for risk stratification in primary prostate cancer. European Journal of Nuclear Medicine and Molecular Imaging, 2021, 48, 340-349.	3.3	84
31	Automated Segmentation of Baseline Metabolic Total Tumor Burden in Diffuse Large B-Cell Lymphoma: Which Method Is Most Successful? A Study on Behalf of the PETRA Consortium. Journal of Nuclear Medicine, 2021, 62, 332-337.	2.8	53
32	Adherence to pretreatment and intratreatment imaging of head and neck squamous cell carcinoma patients undergoing (chemo) radiotherapy in a research setting. Clinical Imaging, 2021, 69, 82-90.	0.8	10
33	The Role of ⁸⁹ Zr-Immuno-PET in Navigating and Derisking the Development of Biopharmaceuticals. Journal of Nuclear Medicine, 2021, 62, 438-445.	2.8	39
34	Kinetics and 28-day test–retest repeatability and reproducibility of [¹¹ C]UCB-J PET brain imaging. Journal of Cerebral Blood Flow and Metabolism, 2021, 41, 1338-1350.	2.4	14
35	Advanced analytics and artificial intelligence in gastrointestinal cancer: a systematic review of radiomics predicting response to treatment. European Journal of Nuclear Medicine and Molecular Imaging, 2021, 48, 1785-1794.	3.3	32
36	Clinically feasible semi-automatic workflows for measuring metabolically active tumour volume in metastatic melanoma. European Journal of Nuclear Medicine and Molecular Imaging, 2021, 48, 1498-1510.	3.3	4

#	Article	IF	CITATIONS
37	Classification of negative and positive 18F-florbetapir brain PET studies in subjective cognitive decline patients using a convolutional neural network. European Journal of Nuclear Medicine and Molecular Imaging, 2021, 48, 721-728.	3.3	16
38	[18F]FDG Uptake in Adipose Tissue Is Not Related to Inflammation in Type 2 Diabetes Mellitus. Molecular Imaging and Biology, 2021, 23, 117-126.	1.3	8
39	Multiparametric functional MRI and 18F-FDG-PET for survival prediction in patients with head and neck squamous cell carcinoma treated with (chemo)radiation. European Radiology, 2021, 31, 616-628.	2.3	33
40	Effect of Shortening the Scan Duration on Quantitative Accuracy of [18F]Flortaucipir Studies. Molecular Imaging and Biology, 2021, 23, 604-613.	1.3	10
41	Feasibility of pharmacokinetic parametric PET images in scaled subprofile modelling using principal component analysis. NeuroImage: Clinical, 2021, 30, 102625.	1.4	4
42	SUVs Are Adequate Measures of Lesional ¹⁸ F-DCFPyL Uptake in Patients with Low Prostate Cancer Disease Burden. Journal of Nuclear Medicine, 2021, 62, 1264-1269.	2.8	2
43	Arterial wall inflammation is increased in rheumatoid arthritis compared with osteoarthritis, as a marker of early atherosclerosis. Rheumatology, 2021, 60, 3360-3368.	0.9	18
44	Non-invasive Standardised Uptake Value for Verification of the Use of Previously Validated Reference Region for [18F]Flortaucipir and [18F]Florbetapir Brain PET Studies. Molecular Imaging and Biology, 2021, 23, 550-559.	1.3	2
45	Harmonisation of PET/CT contrast recovery performance for brain studies. European Journal of Nuclear Medicine and Molecular Imaging, 2021, 48, 2856-2870.	3.3	22
46	In vivo tau pathology is associated with synaptic loss and altered synaptic function. Alzheimer's Research and Therapy, 2021, 13, 35.	3.0	47
47	Use of population input functions for reduced scan duration whole-body Patlak 18F-FDG PET imaging. EJNMMI Physics, 2021, 8, 11.	1.3	17
48	Plausibility and redundancy analysis to select FDGâ€₽ET textural features in nonâ€small cell lung cancer. Medical Physics, 2021, 48, 1226-1238.	1.6	15
49	Amyloid burden quantification depends on PET and MR image processing methodology. PLoS ONE, 2021, 16, e0248122.	1.1	5
50	Interobserver Agreement on Automated Metabolic Tumor Volume Measurements of Deauville Score 4 and 5 Lesions at Interim ¹⁸ F-FDG PET in Diffuse Large B-Cell Lymphoma. Journal of Nuclear Medicine, 2021, 62, 1531-1536.	2.8	8
51	Dynamic PET image reconstruction utilizing intrinsic dataâ€driven HYPR4D denoising kernel. Medical Physics, 2021, 48, 2230-2244.	1.6	15
52	Quantitative PET in the 2020s: a roadmap. Physics in Medicine and Biology, 2021, 66, 06RM01.	1.6	36
53	Arterial wall inflammation in rheumatoid arthritis is reduced by anti-inflammatory treatment. Seminars in Arthritis and Rheumatism, 2021, 51, 457-463.	1.6	9
54	Strategies to reduce sample sizes in Alzheimer's disease primary and secondary prevention trials using longitudinal amyloid PET imaging. Alzheimer's Research and Therapy, 2021, 13, 82.	3.0	14

#	Article	IF	CITATIONS
55	Moving the goalposts while scoring―the dilemma posed by new PET technologies. European Journal of Nuclear Medicine and Molecular Imaging, 2021, 48, 2696-2710.	3.3	13
56	A dual-time-window protocol to reduce acquisition time of dynamic tau PET imaging using [18F]MK-6240. EJNMMI Research, 2021, 11, 49.	1.1	9
57	Spatial concordance of DNA methylation classification in diffuse glioma. Neuro-Oncology, 2021, 23, 2054-2065.	0.6	19
58	Optimal timing and criteria of interim PET in DLBCL: a comparative study of 1692 patients. Blood Advances, 2021, 5, 2375-2384.	2.5	40
59	Head-to-head comparison of (R)-[11C]verapamil and [18F]MC225 in non-human primates, tracers for measuring P-glycoprotein function. European Journal of Nuclear Medicine and Molecular Imaging, 2021, 48, 4307-4317.	3.3	6
60	Performance of nanoScan PET/CT and PET/MR for quantitative imaging of 18F and 89Zr as compared with ex vivo biodistribution in tumor-bearing mice. EJNMMI Research, 2021, 11, 57.	1.1	6
61	Evaluation of P-glycoprotein function at the blood–brain barrier using [18F]MC225-PET. European Journal of Nuclear Medicine and Molecular Imaging, 2021, 48, 4105-4106.	3.3	7
62	[¹⁸ F]Flortaucipir PET Across Various <i>MAPT</i> Mutations in Presymptomatic and Symptomatic Carriers. Neurology, 2021, 97, e1017-e1030.	1.5	16
63	The approval of a disease-modifying treatment for Alzheimer's disease: impact and consequences for the nuclear medicine community. European Journal of Nuclear Medicine and Molecular Imaging, 2021, 48, 3033-3036.	3.3	6
64	Biodistribution of ¹⁸ F-FES in patients with metastatic ER+ breast cancer undergoing treatment with Rintodestrant (G1T48), a novel selective estrogen receptor degrader. Journal of Nuclear Medicine, 2021, , jnumed.121.262500.	2.8	2
65	Potential and pitfalls of 89Zr-immuno-PET to assess target status: 89Zr-trastuzumab as an example. EJNMMI Research, 2021, 11, 74.	1.1	6
66	Aberrant patterns of PET response during treatment for DLBCL patients with MYC gene rearrangements. European Journal of Nuclear Medicine and Molecular Imaging, 2021, , 1.	3.3	4
67	Incorporating radiomics into clinical trials: expert consensus endorsed by the European Society of Radiology on considerations for data-driven compared to biologically driven quantitative biomarkers. European Radiology, 2021, 31, 6001-6012.	2.3	53
68	Repeatability of IVIM biomarkers from diffusionâ€weighted MRI in head and neck: Bayesian probability versus neural network. Magnetic Resonance in Medicine, 2021, 85, 3394-3402.	1.9	19
69	Repeatability of two semi-automatic artificial intelligence approaches for tumor segmentation in PET. EJNMMI Research, 2021, 11, 4.	1.1	15
70	Pharmacokinetic Modeling of (<i>R</i>)-[¹¹ C]verapamil to Measure the P-Glycoprotein Function in Nonhuman Primates. Molecular Pharmaceutics, 2021, 18, 416-428.	2.3	3
71	Diagnostic Performance of [18F]FDG PET in Staging Grade 1–2, Estrogen Receptor Positive Breast Cancer. Diagnostics, 2021, 11, 1954.	1.3	10
72	Reply: Automated Segmentation of TMTV in DLBCL Patients: What About Method Measurement Uncertainty?. Journal of Nuclear Medicine, 2021, 62, 432-432.	2.8	2

#	Article	IF	CITATIONS
73	A systematic review and quality of reporting checklist for repeatability and reproducibility of radiomic features. Physics and Imaging in Radiation Oncology, 2021, 20, 69-75.	1.2	37
74	Bone Metastases Are Measurable: The Role of Whole-Body MRI and Positron Emission Tomography. Frontiers in Oncology, 2021, 11, 772530.	1.3	14
75	Longitudinal [¹⁸ F]flortaucipir PET: Comparison of quantitative and semiâ€quantitative parameters. Alzheimer's and Dementia, 2021, 17, .	0.4	0
76	Quantitative parametric maps of O-(2-[¹⁸ F]fluoroethyl)-L-tyrosine kinetics in diffuse glioma. Journal of Cerebral Blood Flow and Metabolism, 2020, 40, 895-903.	2.4	8
77	Parametric methods for [¹⁸ F]flortaucipir PET. Journal of Cerebral Blood Flow and Metabolism, 2020, 40, 365-373.	2.4	22
78	Test–retest repeatability of [¹⁸ F]Flortaucipir PET in Alzheimer's disease and cognitively normal individuals. Journal of Cerebral Blood Flow and Metabolism, 2020, 40, 2464-2474.	2.4	23
79	Improved detection of diffuse glioma infiltration with imaging combinations: a diagnostic accuracy study. Neuro-Oncology, 2020, 22, 412-422.	0.6	59
80	Image Quality and Activity Optimization in Oncologic ¹⁸ F-FDG PET Using the Digital Biograph Vision PET/CT System. Journal of Nuclear Medicine, 2020, 61, 764-771.	2.8	41
81	Experimental Multicenter and Multivendor Evaluation of the Performance of PET Radiomic Features Using 3-Dimensionally Printed Phantom Inserts. Journal of Nuclear Medicine, 2020, 61, 469-476.	2.8	54
82	Image Quality and Semiquantitative Measurements on the Biograph Vision PET/CT System: Initial Experiences and Comparison with the Biograph mCT. Journal of Nuclear Medicine, 2020, 61, 129-135.	2.8	56
83	Lesion Detection and Interobserver Agreement with Advanced Image Reconstruction for ¹⁸ F-DCFPyL PET/CT in Patients with Biochemically Recurrent Prostate Cancer. Journal of Nuclear Medicine, 2020, 61, 210-216.	2.8	10
84	[89Zr]Zr-cetuximab PET/CT as biomarker for cetuximab monotherapy in patients with RAS wild-type advanced colorectal cancer. European Journal of Nuclear Medicine and Molecular Imaging, 2020, 47, 849-859.	3.3	22
85	Letter to the Editor re: Semiquantitative Parameters in PSMA-Targeted PET Imaging with [18F]DCFPyL: Impact of Tumor Burden on Normal Organ Uptake. Molecular Imaging and Biology, 2020, 22, 15-17.	1.3	7
86	Repeatability of Quantitative ¹⁸ F-DCFPyL PET/CT Measurements in Metastatic Prostate Cancer. Journal of Nuclear Medicine, 2020, 61, 1320-1325.	2.8	22
87	Supporting data for positron emission tomography-based risk modelling using a fixed-instead of a relative thresholding method for total metabolic tumor volume determination. Data in Brief, 2020, 28, 104976.	0.5	1
88	The QIBA Profile for FDG PET/CT as an Imaging Biomarker Measuring Response to Cancer Therapy. Radiology, 2020, 294, 647-657.	3.6	49
89	Hippocampal [18F]flortaucipir BPND corrected for possible spill-in of the choroid plexus retains strong clinico-pathological relationships. NeuroImage: Clinical, 2020, 25, 102113.	1.4	5
90	Why Is Amyloid-β PET Requested After Performing CSF Biomarkers?. Journal of Alzheimer's Disease, 2020, 73, 559-569.	1.2	8

#	Article	IF	CITATIONS
91	Dynamic risk assessment based on positron emission tomography scanning in diffuse large B-cell lymphoma: Post-hoc analysis from the PETAL trial. European Journal of Cancer, 2020, 124, 25-36.	1.3	67
92	Should vascular wall 18F-FDG uptake be adjusted for the extent of atherosclerotic burden?. International Journal of Cardiovascular Imaging, 2020, 36, 545-551.	0.7	2
93	The Additional Value of Ultrafast DCE-MRI to DWI-MRI and 18F-FDG-PET to Detect Occult Primary Head and Neck Squamous Cell Carcinoma. Cancers, 2020, 12, 2826.	1.7	10
94	Multitracer model for staging cortical amyloid deposition using PET imaging. Neurology, 2020, 95, e1538-e1553.	1.5	55
95	Pharmacokinetic Modeling of [18F]MC225 for Quantification of the P-Glycoprotein Function at the Blood–Brain Barrier in Non-Human Primates with PET. Molecular Pharmaceutics, 2020, 17, 3477-3486.	2.3	14
96	In vivo tracking of single cells with PET. Nature Biomedical Engineering, 2020, 4, 765-766.	11.6	6
97	COVID-19 and the brain: impact on nuclear medicine in neurology. European Journal of Nuclear Medicine and Molecular Imaging, 2020, 47, 2487-2492.	3.3	18
98	Tau PET and relative cerebral blood flow in dementia with Lewy bodies: A PET study. NeuroImage: Clinical, 2020, 28, 102504.	1.4	14
99	Earlyâ€onset Alzheimer's disease is related to differential spatial patterns of tau pathology and cognitive impairment. Alzheimer's and Dementia, 2020, 16, e042041.	0.4	0
100	Quantitative accuracy remains after shortening of dynamic [18 F]flortaucipir PET protocol. Alzheimer's and Dementia, 2020, 16, e045710.	0.4	0
101	Regional tau pathology is associated with loss of synapses and reduced synaptic activity: A combined [18 F]flortaucipir, [11 C]UCB†and magnetoencephalography study. Alzheimer's and Dementia, 2020, 16, e045806.	0.4	0
102	Regional distribution of tau pathology in cognitively unimpaired, genetically identical twins. Alzheimer's and Dementia, 2020, 16, e045876.	0.4	0
103	EANM practice guideline/SNMMI procedure standard for dopaminergic imaging in Parkinsonian syndromes 1.0. European Journal of Nuclear Medicine and Molecular Imaging, 2020, 47, 1885-1912.	3.3	134
104	Tau pathology and relative cerebral blood flow are independently associated with cognition in Alzheimer's disease. European Journal of Nuclear Medicine and Molecular Imaging, 2020, 47, 3165-3175.	3.3	28
105	Outcome prediction of head and neck squamous cell carcinoma by MRI radiomic signatures. European Radiology, 2020, 30, 6311-6321.	2.3	49
106	The Image Biomarker Standardization Initiative: Standardized Quantitative Radiomics for High-Throughput Image-based Phenotyping. Radiology, 2020, 295, 328-338.	3.6	1,869
107	Guidelines for the content and format of PET brain data in publications and archives: A consensus paper. Journal of Cerebral Blood Flow and Metabolism, 2020, 40, 1576-1585.	2.4	47
108	Quantification of PD-L1 Expression with ¹⁸ F-BMS-986192 PET/CT in Patients with Advanced-Stage Non–Small Cell Lung Cancer. Journal of Nuclear Medicine, 2020, 61, 1455-1460.	2.8	54

#	Article	IF	CITATIONS
109	Optimizing Workflows for Fast and Reliable Metabolic Tumor Volume Measurements in Diffuse Large B Cell Lymphoma. Molecular Imaging and Biology, 2020, 22, 1102-1110.	1.3	32
110	Quantitative Assessment of Arthritis Activity in Rheumatoid Arthritis Patients Using [11C]DPA-713 Positron Emission Tomography. International Journal of Molecular Sciences, 2020, 21, 3137.	1.8	4
111	PET segmentation of bulky tumors: Strategies and workflows to improve inter-observer variability. PLoS ONE, 2020, 15, e0230901.	1.1	17
112	Regional [18F]flortaucipir PET is more closely associated with disease severity than CSF p-tau in Alzheimer's disease. European Journal of Nuclear Medicine and Molecular Imaging, 2020, 47, 2866-2878.	3.3	29
113	Comparison Between the Performance of Quantitative Flow Ratio and PerfusionÂlmaging for Diagnosing Myocardial Ischemia. JACC: Cardiovascular Imaging, 2020, 13, 1976-1985.	2.3	13
114	Baseline and interim PETâ€based outcome prediction in peripheral Tâ€cell lymphoma: A subgroup analysis of the PETAL trial. Hematological Oncology, 2020, 38, 244-256.	0.8	18
115	Repeatability of arterial input functions and kinetic parameters in muscle obtained by dynamic contrast enhanced MR imaging of the head and neck. Magnetic Resonance Imaging, 2020, 68, 1-8.	1.0	19
116	18f-FDG PET/CT Baseline Rdiomics Features Improve the Prediction of Treatment Outcome in Diffuse Large B-Cell Lymphoma Patients. Blood, 2020, 136, 27-28.	0.6	1
117	Predictive value of quantitative 18F-FDC-PET radiomics analysis in patients with head and neck squamous cell carcinoma. EJNMMI Research, 2020, 10, 102.	1.1	29
118	Optimization of injected 68Ga-PSMA activity based on list-mode phantom data and clinical validation. EJNMMI Physics, 2020, 7, 20.	1.3	5
119	Ischaemic burden and changes in absolute myocardial perfusion after chronic total occlusion percutaneous coronary intervention. EuroIntervention, 2020, 16, e462-e471.	1.4	18
120	Performance Evaluation of a Semi-automated Method for [18F]FDG Uptake in Abdominal Visceral Adipose Tissue. Molecular Imaging and Biology, 2019, 21, 159-167.	1.3	3
121	Quantification of [¹⁸ F]florbetapir: A test–retest tracer kinetic modelling study. Journal of Cerebral Blood Flow and Metabolism, 2019, 39, 2172-2180.	2.4	22
122	Radiomics in Vulvar Cancer: First Clinical Experience Using ¹⁸ F-FDG PET/CT Images. Journal of Nuclear Medicine, 2019, 60, 199-206.	2.8	22
123	PET/CT and PET/MR Tomographs: Image Acquisition and Processing. , 2019, , 199-217.		1
124	Direct comparison of [11C] choline and [18F] FET PET to detect glioma infiltration: a diagnostic accuracy study in eight patients. EJNMMI Research, 2019, 9, 57.	1.1	8
125	Diagnostic performance of regional cerebral blood flow images derived from dynamic PIB scans in Alzheimer's disease. EJNMMI Research, 2019, 9, 59.	1.1	19
126	Factors affecting the harmonization of diseaseâ€related metabolic brain pattern expression quantification in [¹⁸ F]FDGâ€PET (PETMETPAT). Alzheimer's and Dementia: Diagnosis, Assessment and Disease Monitoring, 2019, 11, 472-482.	1.2	13

RONALD BOELLAARD

#	Article	IF	CITATIONS
127	Associations between quantitative [18F]flortaucipir tau PET and atrophy across the Alzheimer's disease spectrum. Alzheimer's Research and Therapy, 2019, 11, 60.	3.0	40
128	Visceral adipose tissue volume is associated with premature atherosclerosis in early type 2 diabetes mellitus independent of traditional risk factors. Atherosclerosis, 2019, 290, 87-93.	0.4	20
129	Impact of Specific Crossing Techniques in Chronic Total Occlusion Percutaneous Coronary Intervention on Recovery of Absolute Myocardial Perfusion. Circulation: Cardiovascular Interventions, 2019, 12, e008064.	1.4	11
130	Exploring effects of Souvenaid on cerebral glucose metabolism in Alzheimer's disease. Alzheimer's and Dementia: Translational Research and Clinical Interventions, 2019, 5, 492-500.	1.8	5
131	Repeatability of [18F]FDG PET/CT total metabolic active tumour volume and total tumour burden in NSCLC patients. EJNMMI Research, 2019, 9, 14.	1.1	26
132	Partial-volume correction in dynamic PET-CT: effect on tumor kinetic parameter estimation and validation of simplified metrics. EJNMMI Research, 2019, 9, 12.	1.1	12
133	Sensitivity of 18F-fluorodihydrotestosterone PET-CT to count statistics and reconstruction protocol in metastatic castration-resistant prostate cancer. EJNMMI Research, 2019, 9, 70.	1.1	10
134	Optimization of parathyroid 11C-choline PET protocol for localization of parathyroid adenomas in patients with primary hyperparathyroidism. EJNMMI Research, 2019, 9, 73.	1.1	15
135	Validated imaging biomarkers as decision-making tools in clinical trials and routine practice: current status and recommendations from the EIBALL* subcommittee of the European Society of Radiology (ESR). Insights Into Imaging, 2019, 10, 87.	1.6	61
136	Metabolic Biomarker–Based BRAFV600 Mutation Association and Prediction in Melanoma. Journal of Nuclear Medicine, 2019, 60, 1545-1552.	2.8	19
137	Discordant amyloid-β PET and CSF biomarkers and its clinical consequences. Alzheimer's Research and Therapy, 2019, 11, 78.	3.0	40
138	Clinically Valuable Quality Control for PET/MRI Systems: Consensus Recommendation From the HYBRID Consortium. Frontiers in Physics, 2019, 7, .	1.0	12
139	Relative cerebral flow from dynamic PIB scans as an alternative for FDG scans in Alzheimer's disease PET studies. PLoS ONE, 2019, 14, e0211000.	1.1	33
140	Interobserver reproducibility of tumor uptake quantification with 89Zr-immuno-PET: a multicenter analysis. European Journal of Nuclear Medicine and Molecular Imaging, 2019, 46, 1840-1849.	3.3	11
141	A new perspective for advanced positron emission tomography–based molecular imaging in neurodegenerative proteinopathies. Alzheimer's and Dementia, 2019, 15, 1081-1103.	0.4	16
142	Task Group 174 Report: Utilization of [18 F]Fluorodeoxyglucose Positron Emission Tomography ([18) Tj ETQqQ	0 0 rgBT 1.6	Overlock 10
143	⁸⁹ Zr-Immuno-PET: Toward a Noninvasive Clinical Tool to Measure Target Engagement of Therapeutic Antibodies In Vivo. Journal of Nuclear Medicine, 2019, 60, 1825-1832.	2.8	38

144Simplified Methods for Quantification of ¹⁸F-DCFPyL Uptake in Patients with Prostate
Cancer. Journal of Nuclear Medicine, 2019, 60, 1730-1735.2.832

#	Article	IF	CITATIONS
145	Tumour necrosis as assessed with 18F-FDG PET is a potential prognostic marker in diffuse large B cell lymphoma independent of MYC rearrangements. European Radiology, 2019, 29, 6018-6028.	2.3	6
146	Binding characterization of N â€(2â€chloroâ€5â€thiomethylphenyl)―N ′â€(3â€[3 H] 3 methoxy phenyl)―N ′â€methylguanidine ([3 H] GMOM), a nonâ€competitive N â€methylâ€Dâ€aspartate (NMDA) receptor antag Pharmacology Research and Perspectives, 2019, 7, e00458.		3
147	Predictive value of quantitative diffusion-weighted imaging and 18-F-FDG-PET in head and neck squamous cell carcinoma treated by (chemo)radiotherapy. European Journal of Radiology, 2019, 113, 39-50.	1.2	38
148	Quantitative assessment of 18F-FDG PET in patients with Hodgkin lymphoma. Nuclear Medicine Communications, 2019, 40, 249-257.	0.5	10
149	RaCaT: An open source and easy to use radiomics calculator tool. PLoS ONE, 2019, 14, e0212223.	1.1	60
150	Optimization of the k2′ Parameter Estimation for the Pharmacokinetic Modeling of Dynamic PIB PET Scans Using SRTM2. Frontiers in Physics, 2019, 7, .	1.0	7
151	P1.04-12 Tumor Uptake and Biodistribution of 89Zr-Labeled Pembrolizumab in Patients with Metastatic Non-Small-Cell Lung Cancer. Journal of Thoracic Oncology, 2019, 14, S443.	0.5	3
152	Interlesional Heterogeneity of Metastatic Neuroendocrine Tumors Based on 18F-DOPA PET/CT. Clinical Nuclear Medicine, 2019, 44, 612-619.	0.7	3
153	PET and CSF amyloid-β status are differently predicted by patient features: information from discordant cases. Alzheimer's Research and Therapy, 2019, 11, 100.	3.0	21
154	Variability and Repeatability of Quantitative Uptake Metrics in ¹⁸ F-FDG PET/CT of Non–Small Cell Lung Cancer: Impact of Segmentation Method, Uptake Interval, and Reconstruction Protocol. Journal of Nuclear Medicine, 2019, 60, 600-607.	2.8	16
155	Recovery of myocardial perfusion after percutaneous coronary intervention of chronic total occlusions is comparable to hemodynamically significant nonâ€occlusive lesions. Catheterization and Cardiovascular Interventions, 2019, 93, 1059-1066.	0.7	18
156	Functional imaging early during (chemo)radiotherapy for response prediction in head and neck squamous cell carcinoma; a systematic review. Oral Oncology, 2019, 88, 75-83.	0.8	43
157	Multicenter <scp>CT</scp> phantoms public dataset for radiomics reproducibility tests. Medical Physics, 2019, 46, 1512-1518.	1.6	26
158	Performance Characteristics of the Digital Biograph Vision PET/CT System. Journal of Nuclear Medicine, 2019, 60, 1031-1036.	2.8	316
159	Healthy Tissue Uptake of 68Ga-Prostate-Specific Membrane Antigen, 18F-DCFPyL, 18F-Fluoromethylcholine, and 18F-Dihydrotestosterone. Journal of Nuclear Medicine, 2019, 60, 1111-1117.	2.8	23
160	Joint EANM/EANO/RANO practice guidelines/SNMMI procedure standards for imaging of gliomas using PET with radiolabelled amino acids and [18F]FDG: version 1.0. European Journal of Nuclear Medicine and Molecular Imaging, 2019, 46, 540-557.	3.3	348
161	Repeatability of ¹⁸ Fâ€ <scp>FDG PET</scp> radiomic features: A phantom study to explore sensitivity to image reconstruction settings, noise, and delineation method. Medical Physics, 2019, 46, 665-678.	1.6	81
162	Semi-quantitative cerebral blood flow parameters derived from non-invasive [¹⁵ 0]H ₂ 0 PET studies. Journal of Cerebral Blood Flow and Metabolism, 2019, 39, 163-172.	2.4	12

#	Article	IF	CITATIONS
163	The Optimal Timing of Interim 18F-FDG PET in Diffuse Large B-Cell Lymphoma: An Individual Patient Data Meta-Analysis By the Petra Consortium. Blood, 2019, 134, 487-487.	0.6	4
164	Updating PET/CT performance standards and PET/CT interpretation criteria should go hand in hand. EJNMMI Research, 2019, 9, 95.	1.1	7
165	Multicentre quantitative 68Ga PET/CT performance harmonisation. EJNMMI Physics, 2019, 6, 19.	1.3	15
166	Quantitative implications of the updated EARL 2019 PET–CT performance standards. EJNMMI Physics, 2019, 6, 28.	1.3	37
167	Inter-site variability of quality control procedures and NEMA image quality in PET/MRI systems. , 2019, 58, .		Ο
168	Baseline Metabolic Tumor Volume in 18FDG-PET-CT Scans in Classical Hodgkin Lymphoma Using Semi-Automatic Segmentation. Blood, 2019, 134, 4049-4049.	0.6	1
169	Feasibility of state of the art PET/CT systems performance harmonisation. European Journal of Nuclear Medicine and Molecular Imaging, 2018, 45, 1344-1361.	3.3	100
170	Does PET Reconstruction Method Affect Deauville Scoring in Lymphoma Patients?. Journal of Nuclear Medicine, 2018, 59, 1167-1169.	2.8	32
171	Reply: Should we assess repeatability of PET quantitative uptake measurements of each 18F-labelled tracer?. European Journal of Nuclear Medicine and Molecular Imaging, 2018, 45, 1274-1275.	3.3	Ο
172	Repeatability of quantitative 18F-FLT uptake measurements in solid tumors: an individual patient data multi-center meta-analysis. European Journal of Nuclear Medicine and Molecular Imaging, 2018, 45, 951-961.	3.3	11
173	Prognostic value of total lesion glycolysis and metabolic active tumor volume in non-small cell lung cancer. Cancer Treatment and Research Communications, 2018, 15, 7-12.	0.7	19
174	Baseline PET as prognostic marker for Hodgkin?. Blood, 2018, 131, 3-4.	0.6	3
175	Validation of [18F]FLT as a perfusion-independent imaging biomarker of tumour response in EGFR-mutated NSCLC patients undergoing treatment with an EGFR tyrosine kinase inhibitor. EJNMMI Research, 2018, 8, 22.	1.1	4
176	Noise-Induced Variability of Immuno-PET with Zirconium-89-Labeled Antibodies: an Analysis Based on Count-Reduced Clinical Images. Molecular Imaging and Biology, 2018, 20, 1025-1034.	1.3	13
177	Prognostic Value of [18 F]-Fluoromethylcholine Positron Emission Tomography/Computed Tomography Before Stereotactic Body Radiation Therapy for Oligometastatic Prostate Cancer. International Journal of Radiation Oncology Biology Physics, 2018, 101, 406-410.	0.4	11
178	Parametric Imaging of [11C]Flumazenil Binding in the Rat Brain. Molecular Imaging and Biology, 2018, 20, 114-123.	1.3	5
179	18F-FDG PET image biomarkers improve prediction of late radiation-induced xerostomia. Radiotherapy and Oncology, 2018, 126, 89-95.	0.3	55
180	EANM/EARL FDG-PET/CT accreditation - summary results from the first 200 accredited imaging systems. European Journal of Nuclear Medicine and Molecular Imaging, 2018, 45, 412-422.	3.3	104

#	Article	IF	CITATIONS
18	Primary tumor volume measurements in Ewing sarcoma: MRI inter- and intraobserver variability and comparison with FDG-PET. Acta OncolÃ ³ gica, 2018, 57, 534-540.	0.8	5
18	² ICâ€Pâ€111: [¹⁸ F]FLORBETAPIRâ€SPECIFIC BINDING IN RELATION TO COGNITION IN SUBJECTIVE COGNITIVE DECLINE. Alzheimer's and Dementia, 2018, 14, P95.	0.4	0
18	³ ICâ€Pâ€222: [18F]AV1451 PET IN RELATION TO ATROPHY ACROSS THE ALZHEIMER'S DISEASE SPECTRUM. Alzheimer's and Dementia, 2018, 14, P180.	0.4	0
184	ICâ€Pâ€182: EVENTâ€BASED MODELING OF THE TEMPORAL ORDERING OF REGIONAL βâ€AMYLOID DEPOSITION BRAIN. Alzheimer's and Dementia, 2018, 14, P152.	N IN THE	1
18	P3â€438: PARAMETRIC IMAGING OF [¹⁸ F]FLORBETAPIR: A TESTâ€RETEST STUDY IN HEALTHY SUBJE AND PATIENTS WITH ALZHEIMER'S DISEASE. Alzheimer's and Dementia, 2018, 14, P1281.	CTS 0.4	0
18	 P2â€360: [¹⁸F]AV1451 PET IN RELATION TO ATROPHY ACROSS THE ALZHEIMER'S DISEASE SPECTRUM. Alzheimer's and Dementia, 2018, 14, P827. 	0.4	0
18'	O2â€06â€01: [¹⁸ F]FLORBETAPIR SPECIFIC BINDING IN RELATION TO COGNITION IN SUBJECTIVE COGNITIVE DECLINE. Alzheimer's and Dementia, 2018, 14, P630.	0.4	0
18	8 O2â€09â€05: EXTENSION AND VALIDATION OF AN AMYLOID STAGING MODEL: ASSOCIATIONS WITH CLINICAL MEASURES. Alzheimer's and Dementia, 2018, 14, P643.	0.4	0
18	9 First in human evaluation of [18F]PK-209, a PET ligand for the ion channel binding site of NMDA receptors. EJNMMI Research, 2018, 8, 69.	1.1	9
19	0 Quantification of O-(2-[18F]fluoroethyl)-L-tyrosine kinetics in glioma. EJNMMI Research, 2018, 8, 72.	1.1	14
19	Mapping heterogeneity in glucose uptake in metastatic melanoma using quantitative 18F-FDG PET/CT analysis. EJNMMI Research, 2018, 8, 101.	1.1	18
19:	 P2â€445: EVENTâ€BASED MODELING OF THE TEMPORAL ORDERING OF REGIONAL βâ€AMYLOID DEPOSITION IN BRAIN. Alzheimer's and Dementia, 2018, 14, P887. 	I THE	1
19	3 Dynamic PET Reconstruction Utilizing a Spatiotemporal 4D De-noising Kernel. , 2018, , .		2
194	A novel partial volume correction method for accurate quantification of [18F] flortaucipir in the hippocampus. EJNMMI Research, 2018, 8, 79.	1.1	19
19	5 SMART (SiMulAtion and ReconsTruction) PET: an efficient PET simulation-reconstruction tool. EJNMMI Physics, 2018, 5, 16.	1.3	14
19	 Feasibility of PET/CT system performance harmonisation for quantitative multicentre 89Zr studies. EJNMMI Physics, 2018, 5, 26. 	1.3	18
19'	 89Zr-atezolizumab imaging as a non-invasive approach to assess clinical response to PD-L1 blockade in cancer. Nature Medicine, 2018, 24, 1852-1858. 	15.2	468
19	 Whole body PD-1 and PD-L1 positron emission tomography in patients with non-small-cell lung cancer. Nature Communications, 2018, 9, 4664. 	5.8	331

#	Article	IF	CITATIONS
199	Episodic memory in mild cognitive impairment inversely correlates with the global modularity of the cerebral blood flow network. Psychiatry Research - Neuroimaging, 2018, 282, 73-81.	0.9	7
200	3′-Deoxy-3′-[18F]Fluorothymidine Positron Emission Tomography Depicts Heterogeneous Proliferation Pathology in Idiopathic Pulmonary Arterial Hypertension Patient Lung. Circulation: Cardiovascular Imaging, 2018, 11, e007402.	1.3	14
201	Volume of interest delineation techniques for 18F-FDG PET-CT scans during neoadjuvant extremity soft tissue sarcoma treatment in adults: a feasibility study. EJNMMI Research, 2018, 8, 42.	1.1	3
202	Wholeâ€body parametric PET imaging will replace conventional imageâ€derived PET metrics in clinical oncology. Medical Physics, 2018, 45, 5355-5358.	1.6	6
203	¹⁸ F-FDG-PET uptake in non-infected total hip prostheses. Monthly Notices of the Royal Astronomical Society: Letters, 2018, 89, 634-639.	1.2	12
204	Comparative biodistribution analysis across four different ⁸⁹ Zr-monoclonal antibody tracers—The first step towards an imaging warehouse. Theranostics, 2018, 8, 4295-4304.	4.6	46
205	[1122] Quantitative molecular imaging: Can we trust the SUV?. Physica Medica, 2018, 52, 46.	0.4	0
206	Radiomics analysis of pre-treatment [18F]FDG PET/CT for patients with metastatic colorectal cancer undergoing palliative systemic treatment. European Journal of Nuclear Medicine and Molecular Imaging, 2018, 45, 2307-2317.	3.3	50
207	Whole body PD-L1 PET in patients with NSCLC and melanoma Journal of Clinical Oncology, 2018, 36, 139-139.	0.8	2
208	Crossed Cerebellar Diaschisis in Alzheimer's Disease. Current Alzheimer Research, 2018, 15, 1267-1275.	0.7	13
209	Prediction of disease-free survival using relative change in FDC-uptake early during neoadjuvant chemoradiotherapy for potentially curable esophageal cancer: A prospective cohort study. Ecological Management and Restoration, 2017, 30, 1-7.	0.2	2
210	Altered GABA _A receptor density and unaltered blood–brain barrier [¹¹ C]flumazenil transport in drug-resistant epilepsy patients with mesial temporal sclerosis. Journal of Cerebral Blood Flow and Metabolism, 2017, 37, 97-105.	2.4	8
211	Textural features of 18F-fluorodeoxyglucose positron emission tomography scanning in diagnosing aortic prosthetic graft infection. European Journal of Nuclear Medicine and Molecular Imaging, 2017, 44, 886-894.	3.3	23
212	In Vivo Evaluation of ¹¹ C-Preladenant for PET Imaging of Adenosine A _{2A} Receptors in the Conscious Monkey. Journal of Nuclear Medicine, 2017, 58, 762-767.	2.8	19
213	Pharmacokinetic modeling of [11C]flumazenil kinetics in the rat brain. EJNMMI Research, 2017, 7, 17.	1.1	7
214	Quantification of Tau Load Using [18F]AV1451 PET. Molecular Imaging and Biology, 2017, 19, 963-971.	1.3	42
215	Subtle alterations in cerebrovascular reactivity in mild cognitive impairment detected by graph theoretical analysis and not by the standard approach. NeuroImage: Clinical, 2017, 15, 151-160.	1.4	8
216	EANM/EARL harmonization strategies in PET quantification: from daily practice to multicentre oncological studies. European Journal of Nuclear Medicine and Molecular Imaging, 2017, 44, 17-31.	3.3	206

#	Article	IF	CITATIONS
217	Parametric Method Performance for Dynamic 3′-Deoxy-3′-18F-Fluorothymidine PET/CT in Epidermal Growth Factor Receptor–Mutated Non–Small Cell Lung Carcinoma Patients Before and During Therapy. Journal of Nuclear Medicine, 2017, 58, 920-925.	2.8	4
218	Technical and instrumentational foundations of PET/MRI. European Journal of Radiology, 2017, 94, A3-A13.	1.2	39
219	PET imaging of zirconium-89 labelled cetuximab: A phase I trial in patients with head and neck and lung cancer. Radiotherapy and Oncology, 2017, 122, 267-273.	0.3	48
220	Impact of <scp>PET</scp> / <scp>CT</scp> system, reconstruction protocol, data analysis method, and repositioning on <scp>PET</scp> / <scp>CT</scp> precision: An experimental evaluation using an oncology and brain phantom. Medical Physics, 2017, 44, 6413-6424.	1.6	30
221	Quality assessment of positron emission tomography scans: recommendations for future multicentre trials. Acta OncolĀ ³ gica, 2017, 56, 1459-1464.	0.8	11
222	Androgen and Estrogen Receptor Imaging in Metastatic Breast Cancer Patients as a Surrogate for Tissue Biopsies. Journal of Nuclear Medicine, 2017, 58, 1906-1912.	2.8	48
223	Diagnostic Accuracy of Neuroimaging to Delineate Diffuse Gliomas within the Brain: A Meta-Analysis. American Journal of Neuroradiology, 2017, 38, 1884-1891.	1.2	42
224	Baseline and longitudinal variability of normal tissue uptake values of [18 F]-fluorothymidine-PET images. Nuclear Medicine and Biology, 2017, 51, 18-24.	0.3	4
225	Impact of partial-volume correction in oncological PET studies: a systematic review and meta-analysis. European Journal of Nuclear Medicine and Molecular Imaging, 2017, 44, 2105-2116.	3.3	36
226	Pancreatic Uptake by 18F-FDOPA PET/CT in Patients With Hypoglycemia After Gastric Bypass Surgery Compared With Controls With or Without Carbidopa Pretreatment. Clinical Nuclear Medicine, 2017, 42, 163-168.	0.7	3
227	Quantification, improvement, and harmonization of small lesion detection with state-of-the-art PET. European Journal of Nuclear Medicine and Molecular Imaging, 2017, 44, 4-16.	3.3	156
228	Partial volume correction of brain PET studies using iterative deconvolution in combination with HYPR denoising. EJNMMI Research, 2017, 7, 36.	1.1	21
229	Incorporating HYPR de-noising within iterative PET reconstruction (HYPR-OSEM). Physics in Medicine and Biology, 2017, 62, 6666-6687.	1.6	19
230	[18F]FDG PET/CT-based response assessment of stage IV non-small cell lung cancer treated with paclitaxel-carboplatin-bevacizumab with or without nitroglycerin patches. European Journal of Nuclear Medicine and Molecular Imaging, 2017, 44, 8-16.	3.3	20
231	Parametric Methods for Dynamic 11C-Phenytoin PET Studies. Journal of Nuclear Medicine, 2017, 58, 479-483.	2.8	2
232	Imaging biomarker roadmap for cancer studies. Nature Reviews Clinical Oncology, 2017, 14, 169-186.	12.5	792
233	[P2–387]: EPISODIC MEMORY IN MILD COGNITIVE IMPAIRMENT INVERSELY CORRELATES WITH THE PATIENT CONTRIBUTION TO CEREBRAL BLOOD FLOW NETWORK MODULARITY. Alzheimer's and Dementia, 2017, 13, P777.	0.4	0
234	[P4–235]: PARAMETRIC IMAGING OF TAU LOAD IN ALZHEIMER's PATIENTS AND CONTROLS USING FLORTAUCIPIR. Alzheimer's and Dementia, 2017, 13, P1364.	0.4	0

#	Article	IF	CITATIONS
235	[ICâ€₽â€206]: PARAMETRIC IMAGING OF TAU LOAD IN ALZHEIMER's PATIENTS AND CONTROLS USING FLORTAUCIPIR. Alzheimer's and Dementia, 2017, 13, P150.	0.4	0
236	Reply: Repeatability of Quantitative Whole-Body 18F-FDG PET/CT Uptake Measures in Patients with Non–Small Cell Lung Cancer: Dynamic Versus Test–Retest Design. Journal of Nuclear Medicine, 2017, 58, 1528.2-1529.	2.8	2
237	A MR Guided De-noising for PET Using IHYPR-LR. , 2017, , .		0
238	Performance Improvements in HYPR-OSEM. , 2017, , .		0
239	Variability in quantitative analysis of atherosclerotic plaque inflammation using 18F-FDG PET/CT. PLoS ONE, 2017, 12, e0181847.	1.1	13
240	Vemurafenib plus cobimetinib in unresectable stage IIIc or stage IV melanoma: response monitoring and resistance prediction with positron emission tomography and tumor characteristics (REPOSIT): study protocol of a phase II, open-label, multicenter study. BMC Cancer, 2017, 17, 649.	1.1	12
241	Guidelines for quality control of PET/CT scans in a multicenter clinical study. EJNMMI Physics, 2017, 4, 23.	1.3	17
242	Model selection criteria for dynamic brain PET studies. EJNMMI Physics, 2017, 4, 30.	1.3	18
243	Quality Visits: The EANM/EARL FDG-PET/CT Accreditation Programme. , 2017, , 415-427.		0
244	Standardization of Imaging Biomarkers: The FDG PET/CT Example. , 2017, , 227-240.		1
245	Evaluation of HYPR-OSEM Using Experimental Phantom and Clinical Patient Data. , 2017, , .		0
246	Interaction of quantitative ¹⁸ Fâ€FDCâ€PETâ€CT imaging parameters and human papillomavirus status in oropharyngeal squamous cell carcinoma. Head and Neck, 2016, 38, 529-535.	0.9	23
247	Quantitative agreement between [¹⁵ O]H ₂ O PET and model free QUASAR MRIâ€derived cerebral blood flow and arterial blood volume. NMR in Biomedicine, 2016, 29, 519-526.	1.6	10
248	Investigation of practical initial attenuation image estimates in TOFâ€MLAA reconstruction for PET/MR. Medical Physics, 2016, 43, 4163-4173.	1.6	11
249	In vivo (R)-[11C]PK11195 PET imaging of 18kDa translocator protein in recent onset psychosis. NPJ Schizophrenia, 2016, 2, 16031.	2.0	63
250	Pharmacokinetic modeling of a novel hypoxia PET tracer [18F]HX4 in patients with non-small cell lung cancer. EJNMMI Physics, 2016, 3, 30.	1.3	13
251	Multiparametric Analysis of the Relationship Between Tumor Hypoxia and Perfusion with ¹⁸ F-Fluoroazomycin Arabinoside and ¹⁵ O-H ₂ O PET. Journal of Nuclear Medicine, 2016, 57, 530-535.	2.8	13
252	ICâ€Pâ€196: Quantification of TAU Load Using [¹⁸ F]AVâ€1451 and PET. Alzheimer's and Dementia, 2016, 12, P141.	0.4	0

#	Article	IF	CITATIONS
253	P4â€215: Quantification of Tau Load Using [¹⁸ F]AVâ€1451 and Pet. Alzheimer's and Dementia, 2016, 12, P1109.	0.4	0
254	158P: PET/CT based imaging biomarkers for response prediction of stage IV NSCLC treated with paclitaxel–carboplatin–bevacizumab with or without nitroglycerin. Journal of Thoracic Oncology, 2016, 11, S126-S127.	0.5	0
255	Repeatability of Quantitative Whole-Body ¹⁸ F-FDG PET/CT Uptake Measures as Function of Uptake Interval and Lesion Selection in Non–Small Cell Lung Cancer Patients. Journal of Nuclear Medicine, 2016, 57, 1343-1349.	2.8	53
256	Design of the NLâ€ENIGMA study: Exploring the effect of Souvenaid on cerebral glucose metabolism in early Alzheimer's disease. Alzheimer's and Dementia: Translational Research and Clinical Interventions, 2016, 2, 233-240.	1.8	4
257	Improving the signal-to-noise ratio in static PET reconstruction using HYPR-OSEM. , 2016, , .		1
258	An automatic delineation method for bone marrow absorbed dose estimation in 89Zr PET/CT studies. EJNMMI Physics, 2016, 3, 13.	1.3	2
259	Accurate Delineation of Glioma Infiltration by Advanced PET/MR Neuro-Imaging (FRONTIER Study). Neurosurgery, 2016, 79, 535-540.	0.6	19
260	Parametric Binding Images of the TSPO Ligand ¹⁸ F-DPA-714. Journal of Nuclear Medicine, 2016, 57, 1543-1547.	2.8	23
261	Accuracy and Precision of Partial-Volume Correction in Oncological PET/CT Studies. Journal of Nuclear Medicine, 2016, 57, 1642-1649.	2.8	28
262	Impact of New Scatter Correction Strategies on High-Resolution Research Tomograph Brain PET Studies. Molecular Imaging and Biology, 2016, 18, 627-635.	1.3	3
263	Lungtech, a phase II EORTC trial of SBRT for centrally located lung tumours – a clinical physics perspective. Radiation Oncology, 2016, 11, 7.	1.2	32
264	Quantification of the novel <i>N</i> -methyl- <scp>d</scp> -aspartate receptor ligand [¹¹ C]GMOM in man. Journal of Cerebral Blood Flow and Metabolism, 2016, 36, 1111-1121.	2.4	19
265	Cerebral microglia activation in hepatitis C virus infection correlates to cognitive dysfunction. Journal of Viral Hepatitis, 2016, 23, 348-357.	1.0	39
266	Investigating the state-of-the-art in whole-body MR-based attenuation correction: an intra-individual, inter-system, inventory study on three clinical PET/MR systems. Magnetic Resonance Materials in Physics, Biology, and Medicine, 2016, 29, 75-87.	1.1	62
267	Translation of New Molecular Imaging Approaches to the Clinical Setting: Bridging the Gap to Implementation. Journal of Nuclear Medicine, 2016, 57, 96S-104S.	2.8	8
268	Quantitative and Simplified Analysis of ¹¹ C-Erlotinib Studies. Journal of Nuclear Medicine, 2016, 57, 861-866.	2.8	22
269	The engagement of FDG PET/CT image quality and harmonized quantification: from competitive to complementary. European Journal of Nuclear Medicine and Molecular Imaging, 2016, 43, 1-4.	3.3	41
270	Repeatability of Radiomic Features in Non-Small-Cell Lung Cancer [18F]FDG-PET/CT Studies: Impact of Reconstruction and Delineation. Molecular Imaging and Biology, 2016, 18, 788-795.	1.3	214

#	Article	IF	CITATIONS
271	Repeatability of Quantitative ¹⁸ F-Fluoromethylcholine PET/CT Studies in Prostate Cancer. Journal of Nuclear Medicine, 2016, 57, 721-727.	2.8	22
272	Impact of PET/CT image reconstruction methods and liver uptake normalization strategies on quantitative image analysis. European Journal of Nuclear Medicine and Molecular Imaging, 2016, 43, 249-258.	3.3	49
273	The Association of Glucose Metabolism and Eigenvector Centrality in Alzheimer's Disease. Brain Connectivity, 2016, 6, 1-8.	0.8	18
274	Early 18F-FDG PET/CT Evaluation Shows Heterogeneous Metabolic Responses to Anti-EGFR Therapy in Patients with Metastatic Colorectal Cancer. PLoS ONE, 2016, 11, e0155178.	1.1	4
275	PET Tracers for Imaging of ABC Transporters at the Blood-Brain Barrier: Principles and Strategies. Current Pharmaceutical Design, 2016, 22, 5779-5785.	0.9	24
276	Psychiatric Disorders. , 2016, , 127-138.		0
277	Evaluation of the accuracy of the average Mu-values within patients from MR derived Mu-maps. , 2015, , \cdot		Ο
278	The effect of SUV discretization in quantitative FDC-PET Radiomics: the need for standardized methodology in tumor texture analysis. Scientific Reports, 2015, 5, 11075.	1.6	318
279	Quality control for quantitative multicenter wholeâ€body PET/MR studies: A NEMA image quality phantom study with three current PET/MR systems. Medical Physics, 2015, 42, 5961-5969.	1.6	51
280	Effects of boundary conditions in TOF-MLAA reconstruction for PET/MR. , 2015, , .		0
281	Evaluation of a more optimal initial attenuation image estimate in TOF-MLAA for PET/MR. , 2015, , .		0
282	Challenges of quantification of TSPO in the human brain. Clinical and Translational Imaging, 2015, 3, 403-416.	1.1	16
283	Reply: Simplified Methods for Quantification of ¹⁸ F-Fluoromethylcholine Uptake: Is SUV _{AUC,PP} Actually an SUV?. Journal of Nuclear Medicine, 2015, 56, 1806.2-1807.	2.8	1
284	Neurophysiological Effects of Sleep Deprivation in Healthy Adults, a Pilot Study. PLoS ONE, 2015, 10, e0116906.	1.1	40
285	Metabolically active tumour volume segmentation from dynamic [18F]FLT PET studies in non-small cell lung cancer. EJNMMI Research, 2015, 5, 26.	1.1	2
286	Summary of the UPICT Protocol for ¹⁸ F-FDG PET/CT Imaging in Oncology Clinical Trials. Journal of Nuclear Medicine, 2015, 56, 955-961.	2.8	93
287	Quantification of ¹¹ C-Laniquidar Kinetics in the Brain. Journal of Nuclear Medicine, 2015, 56, 1730-1735.	2.8	5
288	Preclinical evaluation of [18F]PK-209, a new PET ligand for imaging the ion-channel site of NMDA receptors. Nuclear Medicine and Biology, 2015, 42, 205-212.	0.3	21

#	Article	IF	CITATIONS
289	Quantification of ¹⁸ F-Fluorocholine Kinetics in Patients with Prostate Cancer. Journal of Nuclear Medicine, 2015, 56, 365-371.	2.8	32
290	¹⁸ F-FDG or 3′-Deoxy-3′- ¹⁸ F-Fluorothymidine to Detect Transformation of Follicular Lymphoma. Journal of Nuclear Medicine, 2015, 56, 216-221.	2.8	24
291	A Clinical and Experimental Comparison of Time of Flight PET/MRI and PET/CT Systems. Molecular Imaging and Biology, 2015, 17, 714-725.	1.3	10
292	Evaluation of the Effect of Magnetic Field on PET Spatial Resolution and Contrast Recovery Using Clinical PET Scanners and EGSnrc Simulations. IEEE Transactions on Nuclear Science, 2015, 62, 101-110.	1.2	6
293	FDG PET/CT: EANM procedure guidelines for tumour imaging: version 2.0. European Journal of Nuclear Medicine and Molecular Imaging, 2015, 42, 328-354.	3.3	2,188
294	Bias Reduction for Low-Statistics PET: Maximum Likelihood Reconstruction With a Modified Poisson Distribution. IEEE Transactions on Medical Imaging, 2015, 34, 126-136.	5.4	28
295	Quantification of [¹⁸ F]DPA-714 Binding in the Human Brain: Initial Studies in Healthy Controls and Alzheimer'S Disease Patients. Journal of Cerebral Blood Flow and Metabolism, 2015, 35, 766-772.	2.4	99
296	18FDG SUV in the primary tumor and lymph node metastases is not predictive for development of distant metastases in high risk head and neck cancer patients. Oral Oncology, 2015, 51, 536-540.	0.8	3
297	Cerebral perfusion and glucose metabolism in Alzheimer's disease and frontotemporal dementia: two sides of the same coin?. European Radiology, 2015, 25, 3050-3059.	2.3	80
298	Comparison of HRRT and HR+ Scanners for Quantitative (R)-[11C]verapamil, [11C]raclopride and [11C]flumazenil Brain Studies. Molecular Imaging and Biology, 2015, 17, 129-139.	1.3	13
299	Current Image Acquisition Options in PET/MR. Seminars in Nuclear Medicine, 2015, 45, 192-200.	2.5	57
300	Retrospective quality control review of FDG scans in the imaging sub-study of PALETTE EORTC 62072/VEG110727: a randomized, double-blind, placebo-controlled phase III trial. European Journal of Nuclear Medicine and Molecular Imaging, 2015, 42, 848-857.	3.3	25
301	Comparison of Velocity- and Acceleration-Selective Arterial Spin Labeling with [¹⁵ 0]H ₂ 0 Positron Emission Tomography. Journal of Cerebral Blood Flow and Metabolism, 2015, 35, 1296-1303.	2.4	24
302	Quantification of Dynamic ¹¹ C-Phenytoin PET Studies. Journal of Nuclear Medicine, 2015, 56, 1372-1377.	2.8	17
303	PET/CT-Derived Whole-Body and Bone Marrow Dosimetry of ⁸⁹ Zr-Cetuximab. Journal of Nuclear Medicine, 2015, 56, 249-254.	2.8	40
304	89Zr-cetuximab PET imaging in patients with advanced colorectal cancer. Oncotarget, 2015, 6, 30384-30393.	0.8	106
305	Developments in oncological positron emission tomography/computed tomography assessment. Journal of Thoracic Disease, 2015, 7, E637-9.	0.6	0
306	89Zr-immuno-PET for imaging of long circulating drugs and disease targets: why, how and when to be applied?. Quarterly Journal of Nuclear Medicine and Molecular Imaging, 2015, 59, 18-38.	0.4	38

#	Article	IF	CITATIONS
307	Effects of Reusing Baseline Volumes of Interest by Applying (Non-)Rigid Image Registration on Positron Emission Tomography Response Assessments. PLoS ONE, 2014, 9, e87167.	1.1	2
308	Long-term effects of amyloid, hypometabolism, and atrophy on neuropsychological functions. Neurology, 2014, 82, 1768-1775.	1.5	51
309	Validation of simplified dosimetry approaches in 89 Zr-PET/CT: The use of manual versus semi-automatic delineation methods to estimate organ absorbed doses. Medical Physics, 2014, 41, 102503.	1.6	11
310	Repeatability of Metabolically Active Tumor Volume Measurements with FDG PET/CT in Advanced Gastrointestinal Malignancies: A Multicenter Study. Radiology, 2014, 273, 539-548.	3.6	82
311	Amyloid and its association with default network integrity in Alzheimer's disease. Human Brain Mapping, 2014, 35, 779-791.	1.9	37
312	Parametric Methods for Quantification of 18F-FAZA Kinetics in Non–Small Cell Lung Cancer Patients. Journal of Nuclear Medicine, 2014, 55, 1772-1777.	2.8	12
313	Accuracy and precision of pseudo-continuous arterial spin labeling perfusion during baseline and hypercapnia: A head-to-head comparison with 150 H2O positron emission tomography. NeuroImage, 2014, 92, 182-192.	2.1	133
314	Methodological Considerations in Quantification of 3'-Deoxy-3'-[18F]Fluorothymidine Uptake Measured with Positron Emission Tomography in Patients with Non-Small Cell Lung Cancer. Molecular Imaging and Biology, 2014, 16, 136-145.	1.3	8
315	Test-Retest Variability of Various Quantitative Measures to Characterize Tracer Uptake and/or Tracer Uptake Heterogeneity in Metastasized Liver for Patients with Colorectal Carcinoma. Molecular Imaging and Biology, 2014, 16, 13-18.	1.3	21
316	Accurate PET/MR Quantification Using Time of Flight MLAA Image Reconstruction. Molecular Imaging and Biology, 2014, 16, 469-477.	1.3	78
317	18 F-FDG PET standard uptake values of the normal pons in children: establishing a reference value for diffuse intrinsic pontine glioma. EJNMMI Research, 2014, 4, 8.	1.1	4
318	The effect of amyloid pathology and glucose metabolism on cortical volume loss over time in Alzheimer's disease. European Journal of Nuclear Medicine and Molecular Imaging, 2014, 41, 1190-8.	3.3	7
319	Assessment of Simplified Methods to Measure ¹⁸ F-FLT Uptake Changes in EGFR-Mutated Non–Small Cell Lung Cancer Patients Undergoing EGFR Tyrosine Kinase Inhibitor Treatment. Journal of Nuclear Medicine, 2014, 55, 1417-1423.	2.8	17
320	Multicenter Harmonization of ⁸⁹ Zr PET/CT Performance. Journal of Nuclear Medicine, 2014, 55, 264-267.	2.8	63
321	Impact of anatomical and functional severity of coronary atherosclerotic plaques on the transmural perfusion gradient: a [150]H2O PET study. European Heart Journal, 2014, 35, 2094-2105.	1.0	66
322	The need for quantitative PET in multicentre studies. Clinical and Translational Imaging, 2014, 2, 277-280.	1.1	3
323	Pilot study of 89Zr-bevacizumab positron emission tomography in patients with advanced non-small cell lung cancer. EJNMMI Research, 2014, 4, 35.	1.1	43
324	Combined PET/MR: Where Are We Now? Summary Report of the Second International Workshop on PET/MR Imaging April 8–12, 2013, Tubingen, Germany. Molecular Imaging and Biology, 2014, 16, 295-310.	1.3	38

#	Article	IF	CITATIONS
325	Comparison of Simplified Parametric Methods for Visual Interpretation of ¹¹ C-Pittsburgh Compound-B PET Images. Journal of Nuclear Medicine, 2014, 55, 1305-1307.	2.8	24
326	Metabolic activity measured by FDG PET predicts pathological response in locally advanced superior sulcus NSCLC. Lung Cancer, 2014, 85, 205-212.	0.9	23
327	P1-385: RATIONALE AND DESIGN OF THE NL-ENIGMA STUDY, A DUTCH 24-WEEK RANDOMISED CONTROLLED STUDY TO EXPLORE THE EFFECT OF A NUTRITIONAL INTERVENTION ON BRAIN GLUCOSE METABOLISM IN EARLY ALZHEIMER'S DISEASE. , 2014, 10, P455-P456.		0
328	Magnetic field and PET: Does the effect of magnetic field vary with the intrinsic resolution of PET scanners?. , 2014, , .		1
329	IC-P-109: RATIONALE AND DESIGN OF THE NL-ENIGMA STUDY: A DUTCH 24-WEEK RANDOMISED CONTROLLED STUDY TO EXPLORE THE EFFECT OF NUTRITIONAL INTERVENTION ON BRAIN GLUCOSE METABOLISM IN EARLY ALZHEIMER DISEASE. , 2014, 10, P61-P61.		1
330	ImmunoPET imaging with 89Zr-cetuximab in patients with advanced colorectal cancer Journal of Clinical Oncology, 2014, 32, 11102-11102.	0.8	2
331	Positron emission tomography to assess hypoxia and perfusion in lung cancer. World Journal of Clinical Oncology, 2014, 5, 824.	0.9	10
332	MIMEB: A phase II trial to evaluate FDG-PET/FLT-PET, DCE-MRI and molecular biomarkers for early prediction of nonprogression in patients with advanced non-small cell lung cancer treated with erlotinib and bevacizumab Journal of Clinical Oncology, 2014, 32, e19049-e19049.	0.8	0
333	Evaluation of strategies towards harmonization of FDG PET/CT studies in multicentre trials: comparison of scanner validation phantoms and data analysis procedures. European Journal of Nuclear Medicine and Molecular Imaging, 2013, 40, 1507-1515.	3.3	82
334	Reply to: Area under the cumulative SUV-volume histogram is not a viable metric of intratumoral metabolic heterogeneity. European Journal of Nuclear Medicine and Molecular Imaging, 2013, 40, 1469-1470.	3.3	3
335	Pharmacokinetic analysis of [18F]FAZA in non-small cell lung cancer patients. European Journal of Nuclear Medicine and Molecular Imaging, 2013, 40, 1523-1531.	3.3	23
336	Optimisation and harmonisation: two sides of the same coin?. European Journal of Nuclear Medicine and Molecular Imaging, 2013, 40, 982-984.	3.3	9
337	In vivo imaging of the 18-kDa translocator protein (TSPO) with [18F]FEDAA1106 and PET does not show increased binding in Alzheimer's disease patients. European Journal of Nuclear Medicine and Molecular Imaging, 2013, 40, 921-931.	3.3	71
338	EFOMP and EANM: joint recommendations for a curriculum for the education and training of physicists in nuclear medicine. European Journal of Nuclear Medicine and Molecular Imaging, 2013, 40, 645-648.	3.3	0
339	Dopaminergic activity in Tourette syndrome and obsessive-compulsive disorder. European Neuropsychopharmacology, 2013, 23, 1423-1431.	0.3	133
340	Optimized dose regimen for whole-body FDG-PET imaging. EJNMMI Research, 2013, 3, 63.	1,1	73
341	Intervention versus standard medical treatment in patients with symptomatic occlusion of the internal carotid artery: a randomised oxygen-15 PET study. EJNMMI Research, 2013, 3, 79.	1.1	4
342	Microglial activation in Alzheimer's disease: an (R)-[11C]PK11195 positron emission tomography study. Neurobiology of Aging, 2013, 34, 128-136.	1.5	145

#	Article	IF	CITATIONS
343	P.4.032 Neuroinflammation in temporal cortex in schizophrenia patients. European Neuropsychopharmacology, 2013, 23, S93-S94.	0.3	0
344	CTâ€perfusion versus [¹⁵ 0]H ₂ 0 PET in lung tumors: Effects of CTâ€perfusion methodology. Medical Physics, 2013, 40, 052502.	1.6	6
345	Differential effect of <i>APOE</i> genotype on amyloid load and glucose metabolism in AD dementia. Neurology, 2013, 80, 359-365.	1.5	99
346	Stability of FDG-PET Radiomics features: An integrated analysis of test-retest and inter-observer variability. Acta Oncológica, 2013, 52, 1391-1397.	0.8	353
347	Longitudinal Amyloid Imaging Using ¹¹ C-PiB: Methodologic Considerations. Journal of Nuclear Medicine, 2013, 54, 1570-1576.	2.8	148
348	PD-0453: Test-retest repeatability analysis of 18F-FDG PET Radiomics features in NSCLC. Radiotherapy and Oncology, 2013, 106, S176.	0.3	1
349	Limbic and motor circuits involved in symmetry behavior in Tourette's syndrome. CNS Spectrums, 2013, 18, 34-42.	0.7	16
350	Prognostic Impact of [18F]Fluorothymidine and [18F]Fluoro-D-Glucose Baseline Uptakes in Patients with Lung Cancer Treated First-Line with Erlotinib. PLoS ONE, 2013, 8, e53081.	1.1	36
351	Pemetrexed Induced Thymidylate Synthase Inhibition in Non-Small Cell Lung Cancer Patients: A Pilot Study with 3′-Deoxy-3′-[18F]fluorothymidine Positron Emission Tomography. PLoS ONE, 2013, 8, e63705.	1.1	19
352	Mutatis Mutandis: Harmonize the Standard!. Journal of Nuclear Medicine, 2012, 53, 1-3.	2.8	133
353	Amyloid burden and metabolic function in early-onset Alzheimer's disease: parietal lobe involvement. Brain, 2012, 135, 2115-2125.	3.7	109
354	Optimization of Supervised Cluster Analysis for Extracting Reference Tissue Input Curves in (<i>R</i>)-[¹¹ C]PK11195 Brain PET Studies. Journal of Cerebral Blood Flow and Metabolism, 2012, 32, 1600-1608.	2.4	120
355	Repeatability of ¹⁸ F-FDG Uptake Measurements in Tumors: A Metaanalysis. Journal of Nuclear Medicine, 2012, 53, 701-708.	2.8	149
356	Parametric [11C]flumazenil images. Nuclear Medicine Communications, 2012, 33, 422-430.	0.5	9
357	Tumor Lesion Glycolysis and Tumor Lesion Proliferation for Response Prediction and Prognostic Differentiation in Patients With Advanced Non–Small Cell Lung Cancer Treated With Erlotinib. Clinical Nuclear Medicine, 2012, 37, 1058-1064.	0.7	47
358	Integration of FDC- PET/CT into external beam radiation therapy planning. Nuklearmedizin - NuclearMedicine, 2012, 51, 140-153.	0.3	52
359	Comparative Study With New Accuracy Metrics for Target Volume Contouring in PET Image Guided Radiation Therapy. IEEE Transactions on Medical Imaging, 2012, 31, 2006-2024.	5.4	75
360	No Evidence for Additional Blood–Brain Barrier P-Glycoprotein Dysfunction in Alzheimer's Disease Patients with Microbleeds. Journal of Cerebral Blood Flow and Metabolism, 2012, 32, 1468-1471.	2.4	18

#	Article	IF	CITATIONS
361	P-Glycoprotein Function at the Blood–Brain Barrier: Effects of Age and Gender. Molecular Imaging and Biology, 2012, 14, 771-776.	1.3	127
362	O4â€03â€01: Differential impact of apolipoprotein E genotype on distributions of amyloid load and glucose metabolism in Alzheimer's disease. Alzheimer's and Dementia, 2012, 8, P618.	0.4	0
363	Microglial activation in healthy aging. Neurobiology of Aging, 2012, 33, 1067-1072.	1.5	125
364	Quantifying heterogeneity in human tumours using MRI and PET. European Journal of Cancer, 2012, 48, 447-455.	1.3	149
365	EORTC Imaging Group. European Journal of Cancer, Supplement, 2012, 10, 82-87.	2.2	2
366	Assessment of tumour size in PET/CT lung cancer studies: PET- and CT-based methods compared to pathology. EJNMMI Research, 2012, 2, 56.	1.1	57
367	Comparison of oxygen-15 PET and transcranial Doppler CO2-reactivity measurements in identifying haemodynamic compromise in patients with symptomatic occlusion of the internal carotid artery. EJNMMI Research, 2012, 2, 30.	1.1	8
368	Effects of rigid and non-rigid image registration on test-retest variability of quantitative [18F]FDG PET/CT studies. EJNMMI Research, 2012, 2, 10.	1.1	13
369	Bone formation rather than inflammation reflects Ankylosing Spondylitis activity on PET-CT: a pilot study. Arthritis Research and Therapy, 2012, 14, R71.	1.6	49
370	Dual-Phase PET-CT to Differentiate [18F]Fluoromethylcholine Uptake in Reactive and Malignant Lymph Nodes in Patients with Prostate Cancer. PLoS ONE, 2012, 7, e48430.	1.1	33
371	Longitudinal imaging of Alzheimer pathology using [11C]PIB, [18F]FDDNP and [18F]FDG PET. European Journal of Nuclear Medicine and Molecular Imaging, 2012, 39, 990-1000.	3.3	145
372	Predictive value of early and late residual 18F-fluorodeoxyglucose and 18F-fluorothymidine uptake using different SUV measurements in patients with non-small-cell lung cancer treated with erlotinib. European Journal of Nuclear Medicine and Molecular Imaging, 2012, 39, 1117-1127.	3.3	43
373	Reproducibility of quantitative (R)-[11C]verapamil studies. EJNMMI Research, 2012, 2, 1.	1.1	45
374	MIMEB: A phase II trial to evaluate FDG-PET/FLT-PET and DCE-MRI for early prediction of efficacy in patients with advanced non-small cell lung cancer treated with erlotinib and bevacizumab Journal of Clinical Oncology, 2012, 30, 7603-7603.	0.8	0
375	Utility of PET in Pharmaceutical Development. , 2012, , 1-16.		0
376	Need for Standardization of ¹⁸ F-FDG PET/CT for Treatment Response Assessments. Journal of Nuclear Medicine, 2011, 52, 93S-100S.	2.8	137
377	Kinetic analysis in human brain of [11C](R)-rolipram, a positron emission tomographic radioligand to image phosphodiesterase 4: A retest study and use of an image-derived input function. NeuroImage, 2011, 54, 1903-1909.	2.1	36
378	Early Prediction of Nonprogression in Advanced Non–Small-Cell Lung Cancer Treated With Erlotinib By Using [¹⁸ F]Fluorodeoxyglucose and [¹⁸ F]Fluorothymidine Positron Emission Tomography. Journal of Clinical Oncology, 2011, 29, 1701-1708.	0.8	170

#	Article	IF	CITATIONS
379	Quantification of the neurokinin 1 receptor ligand [11C]R116301. Nuclear Medicine Communications, 2011, 32, 896-902.	0.5	4
380	Prediction of functional recovery after revascularization in patients with chronic ischemic myocardial dysfunction. Nuclear Medicine Communications, 2011, 32, 1169-1173.	0.5	2
381	Measurement of metabolic tumor volume: static versus dynamic FDG scans. EJNMMI Research, 2011, 1, 35.	1.1	24
382	Image Derived Input Functions: Effects of Motion on Tracer Kinetic Analyses. Molecular Imaging and Biology, 2011, 13, 25-31.	1.3	12
383	Day-to-Day Test–Retest Variability of CBF, CMRO2, and OEF Measurements Using Dynamic 15O PET Studies. Molecular Imaging and Biology, 2011, 13, 759-768.	1.3	55
384	Measuring response to therapy using FDG PET: semi-quantitative and full kinetic analysis. European Journal of Nuclear Medicine and Molecular Imaging, 2011, 38, 832-842.	3.3	63
385	Evaluation of a cumulative SUV-volume histogram method for parameterizing heterogeneous intratumoural FDG uptake in non-small cell lung cancer PET studies. European Journal of Nuclear Medicine and Molecular Imaging, 2011, 38, 1636-1647.	3.3	163
386	Impact of [18F]FDG PET imaging parameters on automatic tumour delineation: need for improved tumour delineation methodology. European Journal of Nuclear Medicine and Molecular Imaging, 2011, 38, 2136-2144.	3.3	96
387	Increased cerebral (R)-[11C]PK11195 uptake and glutamate release in a rat model of traumatic brain injury: a longitudinal pilot study. Journal of Neuroinflammation, 2011, 8, 67.	3.1	59
388	Widespread and Prolonged Increase in (<i>R</i>)- ¹¹ C-PK11195 Binding After Traumatic Brain Injury. Journal of Nuclear Medicine, 2011, 52, 1235-1239.	2.8	72
389	Standardization of Quantitative Imaging: The Time Is Right, and 18F-FDG PET/CT Is a Good Place to Start. Journal of Nuclear Medicine, 2011, 52, 171-172.	2.8	24
390	Effects of Image Characteristics on Performance of Tumor Delineation Methods: A Test–Retest Assessment. Journal of Nuclear Medicine, 2011, 52, 1550-1558.	2.8	60
391	¹⁸ F-FDG PET as a Tool to Predict the Clinical Outcome of Infliximab Treatment of Rheumatoid Arthritis: An Explorative Study. Journal of Nuclear Medicine, 2011, 52, 77-80.	2.8	104
392	Fluorodeoxyglucose Positron Emission Tomography for Evaluating Early Response During Neoadjuvant Chemoradiotherapy in Patients With Potentially Curable Esophageal Cancer. Annals of Surgery, 2011, 253, 56-63.	2.1	94
393	Quantitative Imaging Test Approval and Biomarker Qualification: Interrelated but Distinct Activities. Radiology, 2011, 259, 875-884.	3.6	80
394	Quantitative Analysis of Response to Treatment with Erlotinib in Advanced Non–Small Cell Lung Cancer Using 18F-FDG and 3′-Deoxy-3′-18F-Fluorothymidine PET. Journal of Nuclear Medicine, 2011, 52, 1871-1877.	2.8	65
395	Image properties of various ML-based reconstructions of very noisy HRRT data. , 2011, , .		3
396	Maximum-likelihood reconstruction based on a modified Poisson distribution to reduce bias in PET. ,		10

³⁹⁶ 2011,,.

#	Article	IF	CITATIONS
397	Myocardial Oxygen Extraction Fraction Measured Using Bolus Inhalation of ¹⁵ O-Oxygen Gas and Dynamic PET. Journal of Nuclear Medicine, 2011, 52, 60-66.	2.8	15
398	Methodological Aspects of Multicenter Studies with Quantitative PET. Methods in Molecular Biology, 2011, 727, 335-349.	0.4	19
399	Image-Derived Input Function for Human Brain Using High Resolution PET Imaging with [11C](R)-rolipram and [11C]PBR28. PLoS ONE, 2011, 6, e17056.	1.1	40
400	Does 18F-Fluorodeoxyglucose Outperform 18F-Fluorothymidine When Using Positron Emission Tomography in Predicting Transformation of Indolent Non-Hodgkin's Lymphoma,. Blood, 2011, 118, 3658-3658.	0.6	0
401	Reduced parahippocampal and lateral temporal GABAA-[11C]flumazenil binding in major depression: preliminary results. European Journal of Nuclear Medicine and Molecular Imaging, 2010, 37, 565-574.	3.3	79
402	FDG PET and PET/CT: EANM procedure guidelines for tumour PET imaging: version 1.0. European Journal of Nuclear Medicine and Molecular Imaging, 2010, 37, 181-200.	3.3	1,147
403	Partial volume correction strategies for quantitative FDG PET in oncology. European Journal of Nuclear Medicine and Molecular Imaging, 2010, 37, 1679-1687.	3.3	128
404	Pharmaceutical preparation of oxygen-15 labelled molecular oxygen and carbon monoxide gasses in a hospital setting. Journal of Clinical Pharmacy and Therapeutics, 2010, 35, 63-69.	0.7	4
405	Arterial Spin Labeling Perfusion MRI at Multiple Delay Times: A Correlative Study with H ₂ ¹⁵ 0 Positron Emission Tomography in Patients with Symptomatic Carotid Artery Occlusion. Journal of Cerebral Blood Flow and Metabolism, 2010, 30, 222-229.	2.4	117
406	<i>In vivo</i> Validation of Reconstruction-Based Resolution Recovery for Human Brain Studies. Journal of Cerebral Blood Flow and Metabolism, 2010, 30, 381-389.	2.4	28
407	Repeatability of Metabolically Active Volume Measurements with ¹⁸ F-FDG and ¹⁸ F-FLT PET in Non–Small Cell Lung Cancer. Journal of Nuclear Medicine, 2010, 51, 1870-1877.	2.8	98
408	Simplified parametric methods for [18F]FDDNP studies. NeuroImage, 2010, 49, 433-441.	2.1	7
409	Influence of ROI definition, partial volume correction and SUV normalization on SUV–survival correlation in oesophageal cancer. Nuclear Medicine Communications, 2010, 31, 652-658.	0.5	18
410	Influence of ROI definition, partial volume correction and SUV normalization on SUV-survival correlation in oesophageal cancer. Nuclear Medicine Communications, 2010, 31, 652-8.	0.5	11
411	Interim positron emission tomography scan in multi-center studies: optimization of visual and quantitative assessments. Leukemia and Lymphoma, 2009, 50, 1748-1749.	0.6	18
412	Radiation Dosimetry of ⁸⁹ Zr-Labeled Chimeric Monoclonal Antibody U36 as Used for Immuno-PET in Head and Neck Cancer Patients. Journal of Nuclear Medicine, 2009, 50, 1828-1836.	2.8	154
413	Relationship of Cerebrospinal Fluid Markers to ¹¹ C-PiB and ¹⁸ F-FDDNP Binding. Journal of Nuclear Medicine, 2009, 50, 1464-1470.	2.8	162
414	Δ9-Tetrahydrocannabinol Induces Dopamine Release in the Human Striatum. Neuropsychopharmacology, 2009, 34, 759-766.	2.8	341

#	Article	IF	CITATIONS
415	Detection of Alzheimer Pathology In Vivo Using Both ¹¹ C-PIB and ¹⁸ F-FDDNP PET. Journal of Nuclear Medicine, 2009, 50, 191-197.	2.8	119
416	Standards for PET Image Acquisition and Quantitative Data Analysis. Journal of Nuclear Medicine, 2009, 50, 11S-20S.	2.8	720
417	HRRT Versus HR+ Human Brain PET Studies: An Interscanner Test–Retest Study. Journal of Nuclear Medicine, 2009, 50, 693-702.	2.8	59
418	Accuracy of 3-Dimensional Reconstruction Algorithms for the High-Resolution Research Tomograph. Journal of Nuclear Medicine, 2009, 50, 72-80.	2.8	40
419	Comparison of transcranial Doppler ultrasonography and positron emission tomography using a three-dimensional template of the middle cerebral artery. Neurological Research, 2009, 31, 52-59.	0.6	13
420	Downregulation of ¹⁸ F-FDG Uptake in PET as an Early Pharmacodynamic Effect in Treatment of Non–Small Cell Lung Cancer with the mTOR Inhibitor Everolimus. Journal of Nuclear Medicine, 2009, 50, 1815-1819.	2.8	29
421	Differential association of [¹¹ C]PIB and [¹⁸ F]FDDNP binding with cognitive impairment. Neurology, 2009, 73, 2079-2085.	1.5	45
422	Reference Tissue Models and Blood–Brain Barrier Disruption: Lessons from (<i>R</i>)-[¹¹ C]PK11195 in Traumatic Brain Injury. Journal of Nuclear Medicine, 2009, 50, 1975-1979.	2.8	24
423	Repeatability of ¹⁸ F-FDG PET in a Multicenter Phase I Study of Patients with Advanced Gastrointestinal Malignancies. Journal of Nuclear Medicine, 2009, 50, 1646-1654.	2.8	129
424	First Evaluation of [11C]R116301 as an In Vivo Tracer of NK1 Receptors in Man. Molecular Imaging and Biology, 2009, 11, 241-245.	1.3	8
425	Evaluation of Tracer Kinetic Models for Analysis of [18F]FDDNP Studies. Molecular Imaging and Biology, 2009, 11, 322-333.	1.3	20
426	Reproducibility of quantitative 18F-3′-deoxy-3′-fluorothymidine measurements using positron emission tomography. European Journal of Nuclear Medicine and Molecular Imaging, 2009, 36, 389-395.	3.3	71
427	Image-derived input functions for PET brain studies. European Journal of Nuclear Medicine and Molecular Imaging, 2009, 36, 463-471.	3.3	51
428	Quantification of (R)-[11C]PK11195 binding in rheumatoid arthritis. European Journal of Nuclear Medicine and Molecular Imaging, 2009, 36, 624-631.	3.3	29
429	Test-retest variability of quantitative [11C]PIB studies in Alzheimer's disease. European Journal of Nuclear Medicine and Molecular Imaging, 2009, 36, 1629-1638.	3.3	62
430	Off-line motion correction methods for multi-frame PET data. European Journal of Nuclear Medicine and Molecular Imaging, 2009, 36, 2002-2013.	3.3	29
431	Hemodynamic changes in ipsi- and contralateral cerebral arterial territories after carotid endarterectomy using positron emission tomography. World Neurosurgery, 2009, 71, 668-676.	1.3	9
432	The Netherlands protocol for standardisation and quantification of FDG whole body PET studies in multi-centre trials. European Journal of Nuclear Medicine and Molecular Imaging, 2008, 35, 2320-2333.	3.3	343

#	Article	IF	CITATIONS
433	18FDG uptake in oesophageal adenocarcinoma: linking biology and outcome. Journal of Cancer Research and Clinical Oncology, 2008, 134, 227-236.	1.2	55
434	NEOadjuvant therapy monitoring with PET and CT in Esophageal Cancer (NEOPEC-trial). BMC Medical Physics, 2008, 8, 3.	2.4	13
435	Noninvasive imaging of macrophages in rheumatoid synovitis using ¹¹ Câ€(<i>R</i>)â€PK11195 and positron emission tomography. Arthritis and Rheumatism, 2008, 58, 3350-3355.	6.7	97
436	Comparison of Plasma Input and Reference Tissue Models for Analysing [¹¹ C]flumazenil Studies. Journal of Cerebral Blood Flow and Metabolism, 2008, 28, 579-587.	2.4	52
437	Imaging trauma in vivo: GABAA benzodiazepine receptor binding. Molecular Psychiatry, 2008, 13, 3-3.	4.1	11
438	Gap Filling Strategies for 3-D-FBP Reconstructions of High-Resolution Research Tomograph Scans. IEEE Transactions on Medical Imaging, 2008, 27, 934-942.	5.4	24
439	Peroperative Neuromonitoring during Carotid Endarterectomy in Relation to Preoperative Positron Emission Tomography Findings. European Journal of Vascular and Endovascular Surgery, 2008, 35, 652-660.	0.8	2
440	Microglia Activation in Recent-Onset Schizophrenia: A Quantitative (R)-[11C]PK11195 Positron Emission Tomography Study. Biological Psychiatry, 2008, 64, 820-822.	0.7	534
441	Reduced GABAA benzodiazepine receptor binding in veterans with post-traumatic stress disorder. Molecular Psychiatry, 2008, 13, 74-83.	4.1	148
442	Partial volume corrected image derived input functions for dynamic PET brain studies: Methodology and validation for [11C]flumazenil. NeuroImage, 2008, 39, 1041-1050.	2.1	127
443	Simplified parametric methods for [11C]PIB studies. NeuroImage, 2008, 42, 76-86.	2.1	85
444	Image derived input functions for dynamic High Resolution Research Tomograph PET brain studies. NeuroImage, 2008, 43, 676-686.	2.1	37
445	Quantitative Issues in Response Measurement by PET. PET Clinics, 2008, 3, 5-11.	1.5	2
446	Comparison of 3D-OP-OSEM and 3D-FBP reconstruction algorithms for High-Resolution Research Tomograph studies: effects of randoms estimation methods. Physics in Medicine and Biology, 2008, 53, 3217-3230.	1.6	34
447	In how many kinetic classes can [¹¹ C]-(R)-PK11195 brain PET data be segmented?. , 2008, , .		0
448	Determinants of coronary microvascular dysfunction in symptomatic hypertrophic cardiomyopathy. American Journal of Physiology - Heart and Circulatory Physiology, 2008, 294, H986-H993.	1.5	101
449	Reproducibility of Tumor Perfusion Measurements Using ¹⁵ O-Labeled Water and PET. Journal of Nuclear Medicine, 2008, 49, 1763-1768.	2.8	44
450	Impact of attenuation correction strategies on the quantification of High Resolution Research Tomograph PET studies. Physics in Medicine and Biology, 2008, 53, 99-118.	1.6	26

#	Article	IF	CITATIONS
451	Importance of fluorodeoxyglucose-positron emission tomography (FDG-PET) and endoscopic ultrasonography parameters in predicting survival following surgery for esophageal cancer. Endoscopy, 2008, 40, 464-471.	1.0	45
452	Impact of wavelet based denoising of â€PK11195 time activity curves on accuracy and precision of kinetic analysis. Medical Physics, 2008, 35, 5069-5078.	1.6	1
453	Implementation of physiological gating on the high resolution research tomograph. , 2008, , .		Ο
454	Performance of a modified supervised cluster algorithm for extracting reference region input functions from (R)-[¹¹ C]PK11195 brain PET studies. , 2008, , .		13
455	Hyperaemic microvascular resistance is not increased in viable myocardium after chronic myocardial infarction. European Heart Journal, 2007, 28, 2320-2325.	1.0	30
456	Microvascular Function in Viable Myocardium After Chronic Infarction Does Not Influence Fractional Flow Reserve Measurements. Journal of Nuclear Medicine, 2007, 48, 1987-1992.	2.8	28
457	SPM analysis of parametric (R)-[11C]PK11195 binding images: Plasma input versus reference tissue parametric methods. NeuroImage, 2007, 35, 1473-1479.	2.1	26
458	Performance evaluation of the ECAT HRRT: an LSO-LYSO double layer high resolution, high sensitivity scanner. Physics in Medicine and Biology, 2007, 52, 1505-1526.	1.6	301
459	Evaluation of Tracer Kinetic Models for Quantification of P-Glycoprotein Function using (R)-[11C]Verapamil and PET. Journal of Cerebral Blood Flow and Metabolism, 2007, 27, 424-433.	2.4	87
460	Quantification of Dopamine Transporter Binding Using [18F]FP-β-CIT and Positron Emission Tomography. Journal of Cerebral Blood Flow and Metabolism, 2007, 27, 1397-1406.	2.4	34
461	Evaluation of Methods for Generating Parametric (R)-[11C]PK11195 Binding Images. Journal of Cerebral Blood Flow and Metabolism, 2007, 27, 1603-1615.	2.4	32
462	Evaluation of Reference Regions for (R)-[11C]PK11195 Studies in Alzheimer's Disease and Mild Cognitive Impairment. Journal of Cerebral Blood Flow and Metabolism, 2007, 27, 1965-1974.	2.4	53
463	Quantification of FDG PET studies using standardised uptake values in multi-centre trials: effects of image reconstruction, resolution and ROI definition parameters. European Journal of Nuclear Medicine and Molecular Imaging, 2007, 34, 392-404.	3.3	268
464	Accuracy of 3D acquisition mode for myocardial FDG PET studies using a BGO-based scanner. European Journal of Nuclear Medicine and Molecular Imaging, 2007, 34, 1439-1446.	3.3	1
465	Influence of Outside Field of View Activity on the Quality of High Resolution Research Tomograph (HRRT) Brain studies. , 2006, , .		4
466	PPET: A software tool for kinetic and parametric analyses of dynamic PET studies. NeuroImage, 2006, 31, T62.	2.1	29
467	Data-driven volume of interest definition: Benefits and pitfalls. NeuroImage, 2006, 31, T63.	2.1	1
468	Performance of Immuno–Positron Emission Tomography with Zirconium-89-Labeled Chimeric Monoclonal Antibody U36 in the Detection of Lymph Node Metastases in Head and Neck Cancer Patients. Clinical Cancer Research, 2006, 12, 2133-2140.	3.2	207

#	Article	IF	CITATIONS
469	Quantitative Experimental Comparison of HRRT versus HR+ PET Brain Studies. , 2006, , .		11
470	Evaluation of Reference Tissue Models for the Analysis of [11C](R)-PK11195 Studies. Journal of Cerebral Blood Flow and Metabolism, 2006, 26, 1431-1441.	2.4	145
471	Impact of Scar on Water-Perfusable Tissue Index in Chronic Ischemic Heart Disease. Molecular Imaging and Biology, 2006, 8, 245-251.	1.3	13
472	Does Myocardial Fibrosis Hinder Contractile Function and Perfusion in Idiopathic Dilated Cardiomyopathy? PET and MR Imaging Study. Radiology, 2006, 240, 380-388.	3.6	51
473	Optimization algorithms and weighting factors for analysis of dynamic PET studies. Physics in Medicine and Biology, 2006, 51, 4217-4232.	1.6	81
474	Monitoring of response to pre-operative chemoradiation in combination with hyperthermia in oesophageal cancer by FDG-PET. International Journal of Hyperthermia, 2006, 22, 149-160.	1.1	47
475	Quantification of subendocardial and subepicardial blood flow using 150-labeled water and PET: experimental validation. Journal of Nuclear Medicine, 2006, 47, 163-72.	2.8	25
476	Measurement of left ventricular volumes and function with O-15–labeled carbon monoxide gated positron emission tomography: Comparison with magnetic resonance imaging. Journal of Nuclear Cardiology, 2005, 12, 639-644.	1.4	19
477	Development of a Tracer Kinetic Plasma Input Model for (R)-[11C]PK11195 Brain Studies. Journal of Cerebral Blood Flow and Metabolism, 2005, 25, 842-851.	2.4	68
478	Effects of ROI definition and reconstruction method on quantitative outcome and applicability in a response monitoring trial. European Journal of Nuclear Medicine and Molecular Imaging, 2005, 32, 294-301.	3.3	247
479	Evaluation of Basis Function and Linear Least Squares Methods for Generating Parametric Blood Flow Images Using 15O-Water and Positron Emission Tomography. Molecular Imaging and Biology, 2005, 7, 273-285.	1.3	101
480	O-145 Prognostic significance of the 18FDG-PET standardized uptake value for inoperable non-small cell lung cancer patients after high-dose radiotherapy. Lung Cancer, 2005, 49, S50.	0.9	4
481	Standardised FDG uptake: A prognostic factor for inoperable non-small cell lung cancer. European Journal of Cancer, 2005, 41, 1533-1541.	1.3	169
482	Multi-input spectral analysis for evaluation of the contribution of radioactive metabolites in (R)-[11C]verapamil PET data. Journal of Cerebral Blood Flow and Metabolism, 2005, 25, S629-S629.	2.4	2
483	Effects of reference tissue versus plasma input parametric kinetic modelling on statistical parametric analysis of [11C](R)-PK11195 binding in Alzheimer's disease (AD) and young and old subjects. Journal of Cerebral Blood Flow and Metabolism, 2005, 25, S643-S643.	2.4	2
484	Comparison of various models for analysing [11C]flumazenil studies. Journal of Cerebral Blood Flow and Metabolism, 2005, 25, S660-S660.	2.4	2
485	Improving accuracy and precision of PET pharmacokinetic analysis using wavelet based denoising of time activity curves. Journal of Cerebral Blood Flow and Metabolism, 2005, 25, S640-S640.	2.4	1
486	Generating parametric binding potential and volume of distribution images using a novel 2D basis function method and the two tissue compartment plasma input model. Journal of Cerebral Blood Flow and Metabolism, 2005, 25, S631-S631.	2.4	0

#	Article	IF	CITATIONS
487	Accuracy and quality of parametric CBF, OEF and CMRO2 images: Effects of fixing parameters. Journal of Cerebral Blood Flow and Metabolism, 2005, 25, S610-S610.	2.4	0
488	Feasibility of deriving CBF, OEF and CMRO2 from a single dynamic PET scan using a short inhalation of oxygen-15 labelled molecular oxygen. Journal of Cerebral Blood Flow and Metabolism, 2005, 25, S671-S671.	2.4	1
489	Delayed contrast enhancement and perfusable tissue index in hypertrophic cardiomyopathy: comparison between cardiac MRI and PET. Journal of Nuclear Medicine, 2005, 46, 923-9.	2.8	24
490	Optimization of attenuation correction for positron emission tomography studies of thorax and pelvis using count-based transmission scans. Physics in Medicine and Biology, 2004, 49, N31-N38.	1.6	12
491	Amygdala activity in obsessive-compulsive disorder with contamination fear: a study with oxygen-15 water positron emission tomography. Psychiatry Research - Neuroimaging, 2004, 132, 225-237.	0.9	98
492	High-quality 124I-labelled monoclonal antibodies for use as PET scouting agents prior to 131I-radioimmunotherapy. European Journal of Nuclear Medicine and Molecular Imaging, 2004, 31, 1645-1652.	3.3	52
493	Correction for emission contamination in transmission scans for the high resolution research tomograph. IEEE Transactions on Nuclear Science, 2004, 51, 673-676.	1.2	9
494	Postinjection transmission scanning in myocardial 18F-FDG PET studies using both filtered backprojection and iterative reconstruction. Journal of Nuclear Medicine, 2004, 45, 169-75.	2.8	12
495	Validation of a multiwell gamma-counter for measuring high-pressure liquid chromatography metabolite profiles. Journal of Nuclear Medicine Technology, 2004, 32, 28-32.	0.4	17
496	Perfusable tissue index as a potential marker of fibrosis in patients with idiopathic dilated cardiomyopathy. Journal of Nuclear Medicine, 2004, 45, 1299-304.	2.8	41
497	Effects of noise, image resolution, and ROI definition on the accuracy of standard uptake values: a simulation study. Journal of Nuclear Medicine, 2004, 45, 1519-27.	2.8	433
498	Quantitative comparison of analytic and iterative reconstruction methods in 2- and 3-dimensional dynamic cardiac 18F-FDG PET. Journal of Nuclear Medicine, 2004, 45, 2008-15.	2.8	34
499	The perfusable tissue index: a marker of myocardial viability. Journal of Nuclear Cardiology, 2003, 10, 684-691.	1.4	21
500	Characterization of a single LSO crystal layer High Resolution Research Tomograph. Physics in Medicine and Biology, 2003, 48, 429-448.	1.6	39
501	Experimental evaluation of iterative reconstruction versus filtered back projection for 3D [150]water PET activation studies using statistical parametric mapping analysis. NeuroImage, 2003, 19, 1170-1179.	2.1	21
502	Attenuation correction of PET activation studies in the presenceof task-related motion. NeuroImage, 2003, 19, 1501-1509.	2.1	21
503	Effects of attenuation correction and reconstruction method on PET activation studies. NeuroImage, 2003, 20, 898-908.	2.1	12
504	Long-Lived Positron Emitters Zirconium-89 and lodine-124 for Scouting of Therapeutic Radioimmunoconjugates with PET. Cancer Biotherapy and Radiopharmaceuticals, 2003, 18, 655-661.	0.7	111

#	Article	IF	CITATIONS
505	(R)- and (S)-[11C]verapamil as PET-tracers for measuring P-glycoprotein function: in vitro and in vivo evaluation. Nuclear Medicine and Biology, 2003, 30, 747-751.	0.3	106
506	Correction methods for missing data in sinograms of the HRRT PET scanner. IEEE Transactions on Nuclear Science, 2003, 50, 1452-1456.	1.2	34
507	Use of an in-field-of-view shield to improve count rate performance of the single crystal layer high-resolution research tomograph PET scanner for small animal brain scans. Physics in Medicine and Biology, 2003, 48, N335-N342.	1.6	5
508	89Zr immuno-PET: comprehensive procedures for the production of 89Zr-labeled monoclonal antibodies. Journal of Nuclear Medicine, 2003, 44, 1271-81.	2.8	264
509	Quantitative 89Zr immuno-PET for in vivo scouting of 90Y-labeled monoclonal antibodies in xenograft-bearing nude mice. Journal of Nuclear Medicine, 2003, 44, 1663-70.	2.8	72
510	Measurement of 18F-FDG concentrations in blood samples: comparison of direct calibration and standard solution methods. Journal of Nuclear Medicine Technology, 2003, 31, 206-9.	0.4	16
511	Matching PET and CT scans of the head and neck area: Development of method and validation. Medical Physics, 2002, 29, 2230-2238.	1.6	29
512	Characteristics of a new fully programmable blood sampling device for monitoring blood radioactivity during PET. European Journal of Nuclear Medicine and Molecular Imaging, 2001, 28, 81-89.	2.2	136
513	Synthesis and pet-studies of (R)-and (S)-[11C]verapamil for measuring PGP function in MDR1A(+/+)/B(+/+) and MDR1A(-/-)/B(-/-) mice. Journal of Labelled Compounds and Radiopharmaceuticals, 2001, 44, S313-S315.	0.5	3
514	Experimental and clinical evaluation of iterative reconstruction (OSEM) in dynamic PET: quantitative characteristics and effects on kinetic modeling. Journal of Nuclear Medicine, 2001, 42, 808-17.	2.8	114
515	Image-derived input functions for determination of MRGlu in cardiac (18)F-FDG PET scans. Journal of Nuclear Medicine, 2001, 42, 1622-9.	2.8	88
516	New Method to Obtain the Midplane Dose Using Portal In Vivo Dosimetry. International Journal of Radiation Oncology Biology Physics, 1998, 41, 465-474.	0.4	83
517	First clinical tests using a liquid-filled electronic portal imaging device and a convolution model for the werification of the midplane dose. Radiotherapy and Oncology, 1998, 47, 303-312.	0.3	62
518	In vivo dosimetry with a liquid-filled electronic portal imaging device. Medical Physics, 1998, 25, 2483-2483.	1.6	2
519	A convolution model to convert transmission dose images to exit dose distributions. Medical Physics, 1997, 24, 189-199.	1.6	61
520	Two-dimensional exit dosimetry using a liquid-filled electronic portal imaging device and a convolution model. Radiotherapy and Oncology, 1997, 44, 149-157.	0.3	53
521	Transmission dosimetry with a liquid-filled electronic portal imaging device. International Journal of Radiation Oncology Biology Physics, 1996, 34, 931-941.	0.4	76
522	The dose response relationship of a liquid-filled electronic portal imaging device. Medical Physics, 1996, 23, 1601-1611.	1.6	50

#	Article	IF	CITATIONS
523	Simulated Annealing in pharmacokinetic modeling of PET neuroreceptor studies: accuracy and precision compared with other optimization algorithms. , 0, , .		1
524	Quantification of dynamic brain studies with the high resolution research tomograph. , 0, , .		3
525	Application of various iterative reconstruction methods for quantitative 3D dynamic brain PET studies. , 0, , .		4
526	High Resolution PET Imaging Characteristics of /sup68/Ga, /sup124/I and /sup 89/Zr Compared to /sup 18/F. , 0, , .		5